Mechanisms of Carbon Dioxide Emissions from Dry Sediments of the River Elbe

Master Thesis

Lelaina Teichert

April 2021

Westfälische Wilhelms-University, Münster
Institute of Landscape Ecology

First supervisor: Prof. Dr. Klaus-Holger Knorr
Second supervisor: Dr. Matthias Koschorreck

Abstract

Enhanced carbon dioxide (CO_2) emissions from drying sediments of streams and rivers, were found to significantly contribute to the global carbon cycle. However, the understanding of the underlying mechanisms controlling the CO_2 emissions from dry sediments is still limited. Focusing on the potential CO_2 sources, microbial respiration and degassing from the groundwater, a variety of methods was applied to study hydrology and the carbon cycling in drying sediments at the river Elbe. Chamber measurements were used to quantify CO_2 emissions and were complemented with a set of methods including incubation experiments, stable carbon analysis ($\delta^{13}C$) and Radon flux measurements (^{222}Rn) to identify sources and mechanisms behind CO_2 emissions from dry river sediments. Average CO_2 fluxes of ~ 148 (± 155) mmol m^{-2} d^{-1} were observed in summer 2020. Additionally, soil moisture and the thickness of the unsaturated zone were found to be good predictors for the CO_2 flux at the study site. For example, the thickness of the unsaturated zone increased the CO_2 flux by ~ 3 mmol m^{-2} d^{-1} per one cm increase of unsaturated zone. The results from ^{222}Rn flux measurements indicated that degassing groundwater is possibly contributing to CO_2 emissions. Yet, quantifications of CO_2 emissions from different sources revealed high production rates of CO_2 from microbial respiration and comparable low CO_2 emissions from groundwater. Even though a high spatial and temporal variability of the data was observed, the gained evidence suggests that microbial respiration is likely to be the main source of CO_2 emissions, whereas CO_2 degassing from the groundwater plays a minor role regarding CO_2 emissions at the study site.

Zusammenfassung

Trockengefallene Sedimente von Bächen und Flüssen emittieren erhöhte Mengen an Kohlenstoffdioxid (CO_2) und tragen so zu den globalen Kohlenstoffemissionen bei. Das Verständnis, welche Mechanismen und Quellen die CO_2-Emissionen aus trockenen Sedimenten steuern, ist jedoch noch begrenzt. Mit dem Fokus auf den potenziellen CO_2-Quellen, mikrobielle Atmung und Ausgasung aus dem Grundwasser, wurde eine Vielzahl von Methoden angewandt, um die Hydrologie und den Kohlenstoffkreislauf in trockengefallenen Sedimenten an der Elbe zu untersuchen. Dafür wurden CO_2-Emissionen mit Haubenmessungen quantifiziert und durch eine Reihe von Methoden, wie Inkubationsexperimenten, Analysen von stabilen Kohlenstoffisotopen ($\delta^{13}C$) und Flussmessungen von Radon (^{222}Rn), ergänzt, um Quellen und Mechanismen der CO_2-Emissionen zu identifizieren. Über den Sommer 2020 wurden durchschnittliche CO_2-Flüsse von ~ 148 (± 155) mmol m^{-2} d^{-1} beobachtet. Des Weiteren konnten Beziehungen zwischen Umweltfaktoren, wie Sedimentfeuchte und der Mächtigkeit des ungesättigten Sedimenthorizontes, und den CO_2-Flüssen ermittelt werden. Es wurde beispielsweise eine Zunahme des CO_2-Flusses um ~ 3 mmol m^{-2} d^{-1} pro cm Zunahme der Mächtigkeit des ungesättigten Sedimentes beobachtet. Ergebnisse der ^{222}Rn-Flussmessungen deuten darauf hin, dass CO_2-Ausgasungen aus dem Grundwasser möglicherweise zu den CO_2-Emissionen beitragen. Abschätzungen der CO_2-Emissionen aus den verschiedenen Quellen zeigten jedoch hohe Produktionsraten von CO_2 aus mikrobieller Atmung und vergleichsweise geringe CO_2-Ausgasung aus dem Grundwasser. Dies deutet darauf hin, dass die CO_2-Emissionen hauptsächlich von mikrobieller Atmung herrühren, während CO_2-Ausgasung aus dem Grundwasser eine untergeordnete Rolle im Hinblick auf die CO_2-Emissionen von trockengefallenen Sedimenten an der Elbe spielen.

Table of Contents

List of Figures V
List of Tables VI
1 Introduction 1
2 Material and methods 4
2.1 Study site 4
2.2 Experimental setup 6
2.2.1 Flux measurements and environmental variables 7
2.2.2 Hydrological measurements 9
2.2.3 Groundwater and river water sampling 9
2.2.4 Stable carbon isotope ($\delta^{13}C$) sampling 9
2.2.5 Radon (^{222}Rn) measurements 10
2.3 Analytical methods 11
2.3.1 Soil samples analysis 11
2.3.2 Incubation experiments 11
2.3.3 Groundwater and river water analysis 12
2.3.4 Stable carbon isotope ($\delta^{13}C$) analysis 12
2.4 Data processing 13
2.4.1 Fluxes and environmental variables 13
2.4.2 Hydrology 13
2.4.3 Incubation experiment and temperature response 14
2.4.4 Chemical equilibrium of groundwater and river water 15
2.4.5 Stable carbon isotopes ($\delta^{13}C$) 17
2.5 Data analysis 17
2.5.1 Fluxes and environmental variables 17
3 Results 20
3.1 Site characteristics 20
3.1.1 Fluxes from dry river sediments 20
3.1.2 Hydrology 22

3.2 The main source of CO_2 emissions 22
3.2.1 Potential of microbial respiration 22
3.2.2 Potential of groundwater evaporation 23
3.2.3 Stable carbon isotope signatures ($\delta^{13}C$) 24
3.2.4 Radon (^{222}Rn) 26
3.3 Influence of environmental variables on the CO_2 flux 27
3.3.1 Automatic measurements 27
3.3.2 Manual measurements 30
4 Discussion 33
4.1 The main source of CO_2 emissions 33
4.2 Influence of environmental variables on the CO_2 flux 36
5 Conclusion 40
Acknowledgment 42
References 43
Appendix 53

List of Figures

Figure 1: The Location of the study site and sampling points 4
Figure 2: Water level changes over the measurement period 5
Figure 3: Experimental setup of the chamber measurements 8
Figure 4: Estimated error of soil moisture from automatic measurements 19
Figure 5: The CO_2 fluxes from automatic measurements 21
Figure 6: The CO_2 fluxes from manual measurements 21
Figure 7: The calculated CO_2 fluxes from incubation experiments compare to CO_2 fluxes measured in the field 22
Figure 8: The temperature response of dry river sediment from Incubation experiment 23
Figure 9: The mean (± SD) $\delta^{13}C$ signatures at the study site for each measurement day 24
Figure 10: The $\delta^{13}C$ signatures at the study site, all measurements summarized by boxplots 25
Figure 11: The CO_2 fluxes and the environmental variables 27
Figure 12: The temperature response of CO_2 fluxes over the measurement period 29
Figure 13: The environmental variables, soil moisture, soil temperature and thickness of the unsaturated zone from the manual measurements, with distance to the river 30
Figure 14: Relationship between CO_2 fluxes and the environmental variables soil moisture and thickness of the unsaturated zone from manual measurements 32
Figure 15: Schematic representation of the study site (cross section) with mechanisms that were found to influence the CO_2 fluxes 39

List of Tables

Table 1: Overview of the methods used in this study together with the aim the methods were applied for 6

Table 2: Summary of measured CO_2 and CH_4 fluxes [mmol m^{-2} d^{-1}], from manual and automatic measurements at the study site 20

Table 3: The estimates of potential groundwater evaporation (E_{GW}) to cover the minimum, average and maximum CO_2 fluxes at the study site 24

Table 4: The ^{222}Rn fluxes at the study site with distance to the river 26

Table 5: The Spearman correlation coefficients of automatically measured data 28

Table 6: The results of soil moisture (θ), loss on ignition (LOI) and bulk density (bd) from soil sample analysis 30

Table 7: The Spearman correlation coefficients of manually measured data 31

Table 8: The results from lmm with the measurement date as a random effect 32

1 Introduction

Streams and rivers are well known to play an important role in the global carbon cycle. The transport of continental carbon to the ocean for example is mainly regulated by rivers (Schlesinger and Melack 1981). Moreover, carbon in rivers undergoes transformation processes and can be stored by means of sedimentation and photosynthesis or released due to biological respiration (Battin et al. 2008; Del Giorgio and Pace 2008). One distinctive feature of rivers is that they are frequently altered by changing water levels. Climate change is expected to increase the seasonal and the inter- annual variability of rivers and hydrological regimes (Coppola et al. 2014; Bolpagni et al. 2019). In Europe, more frequent and longer-lasting droughts are expected during summers, which lead to desiccation of smaller streams and low-water levels in high-order rivers (Steward et al. 2012; Samaniego et al. 2018; Spinoni et al. 2018). Consequently, previously submerged river sediment will be exposed to the atmosphere and influenced by drying (Steward et al. 2012).

Recent studies have shown that exposed sediments from drying inland waters, contribute about 0.12 ± 0.13 PgC yr^{-1} to the global carbon dioxide (CO_2) emissions, which is equivalent to ~ 6 ± 6 % of the CO_2 emissions from inland waters (Keller et al. 2020). High rates of CO_2 emissions from dry sediments are observed for ephemeral streams and small rivers under low-water conditions (e.g. Von Schiller et al. 2014; Gómez-Gener et al. 2015; Looman et al. 2017), whereas estimates for high-order rivers are still scarce (Bolpagni et al. 2019; Mallast et al. 2020). As a first step, Mallast et al. (2020) estimated that for the German part of the River Elbe ~ 6200 - 6600 t yr^{-1} CO_2 were emitted from the exposed sediments during the millennium drought in 2018, highlighting the relevance of drought effects on CO_2 emissions from high-order rivers.

Apart from estimating magnitudes of CO_2 emissions, identifying sources and drivers is likewise of importance to deepen the understanding of regulating mechanisms behind CO_2 emissions from dry sediments (Marcé et al. 2019; Keller et al. 2020). Overall, carbon emissions from any ecosystem, including desiccated sediments, derive from a number of biotic and abiotic sources (Marcé et al. 2019). Respiration from microbial activity is well known to contribute to CO_2 emissions (Weise et al. 2016; Marcé et al. 2019), whereas non-biological processes are rarely taken into account (Rey 2015). Yet, recent findings revealed a spatial dependence of CO_2 fluxes from dry river sediments (Bolpagni et al. 2019; Mallast et al. 2020) that raised the question, how abiotic processes might contribute to CO_2 emissions. As a result, Mallast et al. (2020) suggests that CO_2 from the groundwater is likely to contribute to the CO_2 emissions from sediments alongside high-order rivers. This assumption is based on the mechanism that during

periods of desiccation the water level of the river is falling, while the response of the groundwater level is delayed (Peters et al. 2006). Hence, a flow gradient towards the river is formed resulting in discharge hotspots of groundwater close to the river. Considering that groundwater is usually 10 to 100 fold over-saturated with CO_2 (Macpherson 2009) the dissolved CO_2 degasses when reaching the sediment-atmosphere interface and adds to the CO_2 emissions (Mallast et al. 2020).

After all, the identification of sources and mechanisms behind CO_2 emissions from dry sediments of inland water is challenging (Marcé et al. 2019). Therefore, a complementing set of methods was used in this study, covering the potential CO_2 sources: microbial respiration and degassing from the groundwater. Firstly, incubation experiments of the dry river sediment were performed in the laboratory to determine the potential of microbial respiration and to estimate if CO_2 production rates could cover the measured CO_2 fluxes in the field. Secondly, stable carbon isotope composition was analyzed to investigate the carbon cycling at the study site, including the Keeling plot approach to determine the isotopic composition of the CO_2 flux (Keeling 1958; Cerling et al. 1991; Bowling et al. 2008). Thirdly, the natural occurring geogenic noble gas Radon (^{222}Rn), a product of the decay series of uranium-238 with a half-life time of 3.8 days (Cook and Herczeg 2000), was used as a natural tracer for groundwater influence. Indeed, ^{222}Rn is known to be higher concentrated in groundwater compared to surface water (Genereux et al. 1993; Cook et al. 2008) and moves by the same mass flow and diffusion pathways as other soil gases (Megonigal et al. 2020). Moreover, ^{222}Rn is not affected by biological processes, which makes it altogether a useful tool to trace CO_2 from groundwater and deeper sources (Kim et al. 2020; Megonigal et al. 2020). Furthermore, investigations on how environmental variables are influencing the CO_2 emissions were performed, to gain further insides regarding the CO_2 source. Keller et al. (2020) showed that sediment moisture in combination with organic matter availability and temperature seem to be globally consistent predictors for CO_2 emissions from dry inland waters. Therefore, soil temperature, soil moisture, organic matter and other environmental variables were monitored simultaneously with the CO_2 flux.

This study aimed to identify the main source of CO_2 emissions from dry sediments of the river Elbe to generally improve the understanding of CO_2 emissions from dry river sediments and how they contribute to the global carbon cycle. We assumed that potential main sources of CO_2 emissions from dry sediments at the river Elbe are microbial respiration and degassing groundwater, and hypothesized that I) degassing groundwater is the main source of the CO_2 emissions from the dry sediments of the river Elbe. Supporting the first hypothesis, we further

assume that II) the microbial respiration in the unsaturated zone does not have a considerable influence on the CO_2 emissions, resulting in weak relations between environmental variables like organic matter content and thickness of the unsaturated zone with the CO_2 flux.

2 Material and methods

2.1 Study site

The study site is located at km 314 of the river Elbe, south of Magdeburg, Germany. The River Elbe is one of the largest rivers in Central Europe with a discharge average of about 559 $m^3 s^{-1}$ in Magdeburg (Weigold and Baborowski 2009). Near Magdeburg, the Middle Elbe can be characterized as a free-flowing lowland river with comparable large floodplains, only regulated by groin fields. Hence, seasonal water level fluctuations are shaping the different habitats alongside the river ranging from alluvial forests and pastures to sandy beaches (Scholten et al. 2003; Scholz et al. 2005). The study site is located in between two groins and is characterized by a slight slope from the river to the adjoining floodplain, which extends to ~ 25 m. A sandy beach of about 2 to 5 m with sparse vegetation can be found directly at the river, while the vegetation becomes denser with distance to the river. The adjoining floodplain is used as a cow pasture throughout the whole year.

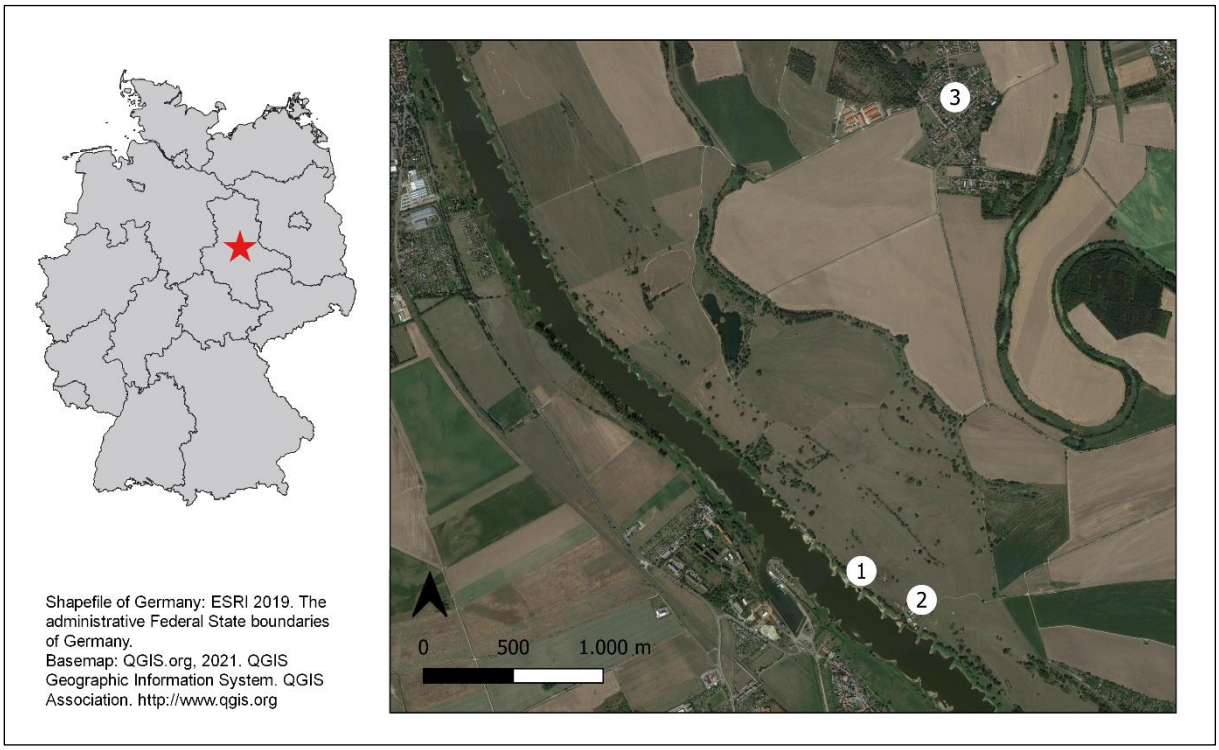

Figure 1: The Location of the study site and sampling points. The study site 1) is located directly at the river Elbe. Sites, where sampling of the distant groundwater in the floodplain took place are highlighted with 2) and 3).

All measurements were performed from the 1st of May till the 7th of October in 2020. During this time automated CO_2 flux measurement devices were set up. Additional sampling campaigns took place from the 3rd of August to the 5th of August, on the 2nd of September, and from the 22nd of September to the 23rd of September. The study site was regularly controlled and monitored in between sampling campaigns. Additional sampling of two groundwater wells in the floodplain of the Elbe took place on the 7th of September in approximately 500 and 2000 m distance to the river Elbe (Fig. 1).

The water level during the campaigns was always below the average low water level (84 cm). The minimum water level over the measurement period was 61 cm on the 24th of September. Whereas the highest water level was on the 26th of June with 223 cm (Fig. 2) (WSV 2020). Compared to 2018 and 2019, the water level was relatively high throughout the whole summer with the highest water level at the end of June. The mean annual temperature is 9.5 °C and the mean annual precipitation is 520 mm, over the reference period of 1981 to 2010 (Deutscher Wetterdienst 2020).

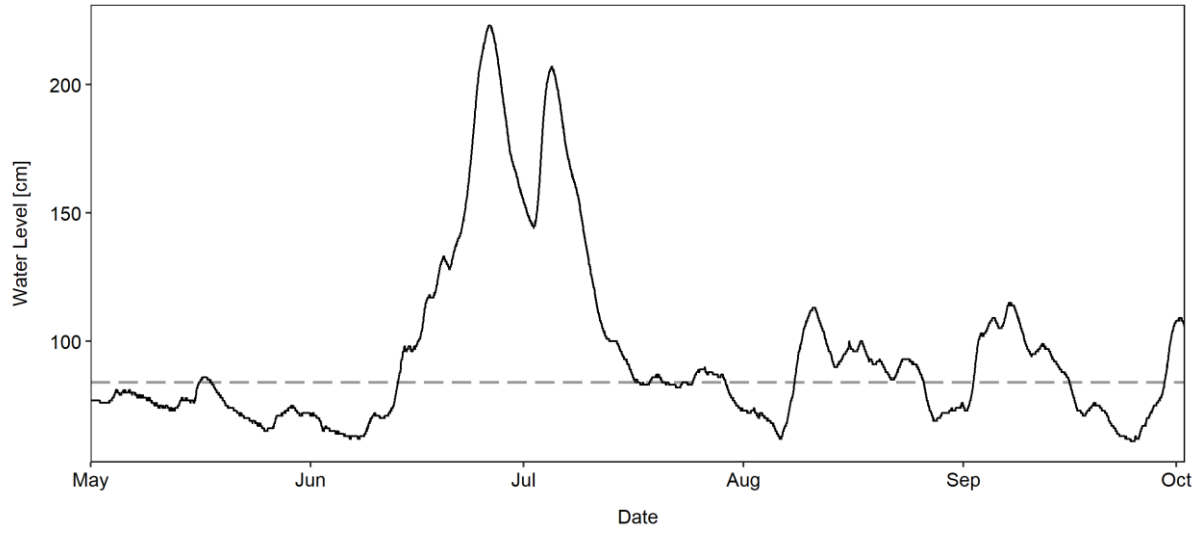

Figure 2: Water level changes over the measurement period, measured at Magdeburger Strombrück ~ 13 km downstream from the study site. The dashed line represents the average low water level of 84 cm.

2.2 Experimental setup

To estimate and identify the magnitude, origins and drivers of the CO_2 emissions from dry sediments at the river Elbe a variety of methods were used. Table 1 provides an overview of the implemented methods together with the aim the methods were applied for. In the following, sampling and analysis methods are described in detail.

Table 1: Overview of the methods used in this study together with the aim the methods were applied for. The methods are categorized by the primary research question.

Research question	Method/ Analysis	Aim
General site characteristics	Chamber measurements	Magnitude and pattern of CO_2 emissions
	Hydraulic conductivity	Characteristics of groundwater movement
	Hydraulic gradient	The direction of the groundwater flow, Formation of groundwater hotspots?
	δ18O, δ2H	Magnitude and pattern of evaporation
Identifying the main source of CO_2 emissions (Hypothesis I)	Incubations of dry river sediment	Potential of microbial respiration including temperature response of microbial respiration
	$\delta^{13}C$, Keeling plots	Investigating carbon-cycling processes, Determining the carbon source
	^{222}Rn	Natural tracer of groundwater influence, Tracing origins or transport of CO_2
Influence of environmental variables on the CO_2 emissions (Hypothesis II)	Sediment analysis	Influence of soil parameters on the CO_2 fluxes
	Environmental variables	Influence of soil temperature, moisture, the thickness of the unsaturated zone and precipitation on the CO_2 fluxes

2.2.1 Flux measurements and environmental variables

To estimate magnitudes and identify spatial and temporal patterns of greenhouse gas emissions at the study site, manual and automatic, closed chamber measurements were performed. For this purpose, sites without vegetation were selected to focus on the two studied CO_2 sources: microbial respiration and CO_2 degassing from groundwater.

The CO_2 fluxes from the dry river sediments were measured with manual chamber measurements during the measurement campaigns in August and September. The manual chamber measurements were performed in 1 m steps away from the flowing water, along a transect which was characterized by an uphill slope of ~ 11.5 %. For the measurements, collars were installed along the transect a day in advance to minimize disturbance during measurements (Fig. 3a). To measure the gas fluxes a chamber (V = 0.0239 m^3, A = 0.1195 m^2) was placed on a collar. Dark and light chamber measurements were performed. The change of concentrations in the chamber was monitored for ~ 5 minutes, with the Multicomponent FTIR gas analyzer (FTIR gas analyzer DX4000, Gasmet Technologies GmbH, Helsinki, Finland). The Multicomponent FTIR gas analyzer measures CO_2, Methane (CH_4) and Nitrous oxide (N_2O) with FTIR spectroscopy, with an accuracy of < 2% of the measuring range per zero-point calibration interval (Gasmet Technologies GmbH 2018). Hence, the detection limit of the CO_2 flux is ~ 2 mmol m^{-2} d^{-1}, while CH_4 flux is detectable if above 0.12 mmol m^{-2} d^{-1} and N_2O if above 0.2 mmol m^{-2} d^{-1}. Additionally, the EGM-5 CO_2 - analyzer with a soil respiration chamber (dark, V = 0.001171 m^3, A = 0.0078 m^2) was used to measure CO_2 fluxes from the sediment, along the transect (EGM-5 Portable CO_2 Gas Analyzer, PP Systems, Amesbury, Massachusetts, USA). Due to easy handling the EGM-5 CO_2 - analyzer was used to monitor CO_2 fluxes at the study site regularly in between the sampling campaigns. The EGM-5 CO_2 - analyzer measurement is based on a non-dispersive infrared (NDIR) measurement technique and measures CO_2 concentration over 2 minutes, with an accuracy of < 1 % over the calibrated range. The described chamber measurements are in following summarized and referred to as manual measurements.

To cover higher temporal dynamics of CO_2 fluxes three dark automatic chambers (CFLUX-1 Automated Soil CO_2 Flux System, PP Systems, Amesbury, Massachusetts, USA), which are in following referred to as automatic measurements, were installed (Fig. 3b). Changes of concentration were measured over 5 minutes once per hour, over a measurement range from 0 – 2000 ppm with an accuracy of < 1% over the calibrated range (PP Systems 2018). The automatic chambers were set up at different distances to the water. The setting was usually that two chambers were placed at the same height, close to the flowing water, while one chamber

was placed further away (Fig. 3b). Due to fluctuating and comparable high-water levels over the summer of 2020 (Fig. 2), it was not possible to measure CO_2 fluxes from the sediment continuously over the whole measurement period. The chambers were set up in the periods from the 1st of Mai to the 10th of June, the 3rd of August to the 6th of August, the 17th of September to the 26th of September, and needed to be moved occasionally. To assure repeatability and comparability of the automatically measured data, fixed positions were estimated. Therefore, the distance of the river and the height over water level were determined once, along the transect. Out of these parameters, a slope was estimated based on linear regression and afterward used to position the automatic chambers in the field. Positions, where the automatic chambers were placed were 75, 85 and 95 cm above zero point of gauge (zero point of gauge = 39.885 m above mean sea level (WSV 2020)).

Complementary to manual and automatic chamber measurements, environmental variables were measured at the study site. Therefore, integrated probes (Stevens HydraProbe, Stevens Water Monitoring Systems, Portland, Oregon, USA) were installed, measuring soil moisture and soil temperature simultaneously with the CO_2 fluxes. The soil temperature sensor measures in a depth of ~ 5 cm and a range from –10 to 55 °C with an accuracy of ± 0.3°C at 25 °C. The soil moisture sensor measures over a depth of ~ 5 cm and a saturation range from 0 to 100 %, depending on the soil characteristics (PP Systems 2020). Furthermore, soil samples were taken along the transect and at the automatic chambers in a depth of 5 cm for incubation analysis in the laboratory. Therefore, four soil samples were taken around a collar for incubation replicates. Additionally, soil samples were taken with a soil sampler (Pürckhauer Set, Eijkelkamp Soil & Water, Giesbeek, The Netherlands) over a depth of ~1 m, visually separated in the unsaturated and saturated zone and later separately analyzed in the laboratory. All soil samples were stored at 4 °C and were a week later analyzed in the laboratory.

a) b)

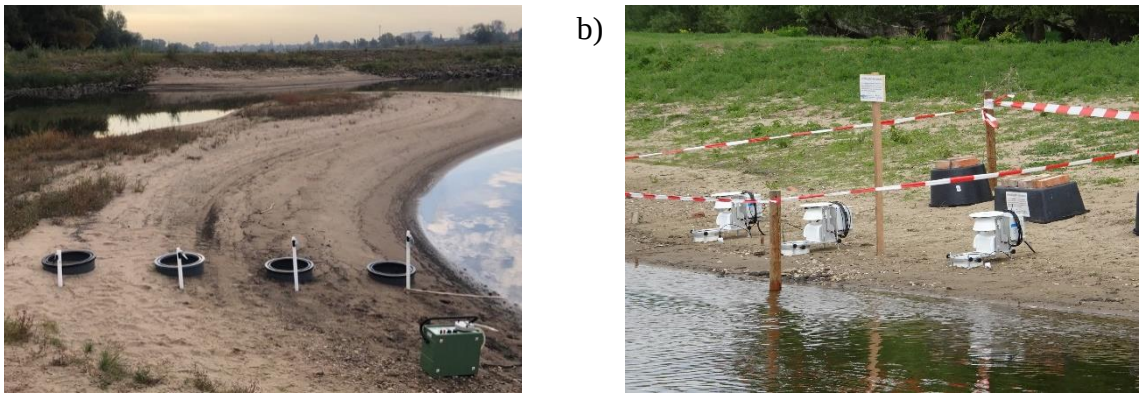

Figure 3: Experimental setup of the chamber measurements. The collars for manual measurement and the piezometers a) were set up along a transect away from the flowing water. The automatic chambers b) were set up at fixed positions in different distances to the flowing water.

2.2.2 Hydrological measurements

The groundwater movement was analyzed during periods of desiccation to identify if the groundwater influences the CO_2 emissions. Therefore, piezometers, with a diameter of 2.7 cm and a length of 100 cm, were installed along the measurement transect, next to the collars (Fig. 3a). The installation of the piezometers and the measurements took place a day before the sampling campaign, to prevent potential errors of further sampling. The hydraulic head of the groundwater (h_{pot}), the water level in the piezometers, was measured with an electric contact gauge, to determine the hydraulic gradient. Additionally, the hydraulic conductivity was measured with the slug test based on (Hvorslev 1951). For that, a level logger (Levelogger 5, Solinst, Georgetown, Ontario, Canada Ltd.) was installed in the piezometer. The piezometer was filled with water and the water level changes were measured till the at-rest water level was reached. This was repeated three times, in each piezometer.

2.2.3 Groundwater and river water sampling

Additional chemical and physical parameters of the groundwater, the river water, and the distant groundwater, were determined to improve the understanding of processes taking place in the saturated zone. Accordingly, values of pH, conductivity, temperature and O_2 saturation were measured in the piezometers, the river and the distant groundwater with a multiparameter probe (WTW® MultiLine® Multi 3630 IDS, Xylem, Rye Brook, New York, USA). To measure CO_2 (aq) and CH_4 (aq) concentrations in the water, water samples were taken from the piezometers and the river using a syringe. Atmospheric air was added, with a headspace ratio of 1:1. By shaking the sample for approximately 2 minutes in the field, headspace equilibrium was adjusted. Afterward, the gas samples were filled in 12 ml evacuated Exetainers (Labco Exetainers®, Labco Limited, Lampeter, UK) and stored till further analysis in the laboratory. Additionally, a CO_2 probe (CO_2 probe, AMT Analysenmesstechnik, Rostock, Germany) was installed in the river in June but due to technical defects, the probe measured only over a short period.

Furthermore, water samples were collected in crimp vials without a headspace, from the piezometer, the river, and the distant groundwater, stored at 4 °C and later analyzed in the laboratory.

2.2.4 Stable carbon isotope ($\delta^{13}C$) sampling

To determine the source of the CO_2 based on its stable isotopic composition, discrete gas samples were taken from the chamber measurements, to derive the source $\delta^{13}CO_2$ signature from Keeling plots (Keeling 1958). Therefore, discrete gas samples were taken from the

chamber measurements. Four gas samples of ~ 20 ml were taken, using a syringe, at regular intervals over a measurement time of 20 – 30 minutes. Additionally, headspace equilibrated gas samples from the ground and the river water were taken, as described in section 2.2.3. All gas samples were filled and stored in evacuated Exetainers till further analysis. For estimation of the $\delta^{13}C$ signatures of organic matter soil samples of the unsaturated zone were taken along the transect with a soil sampler (Pürckhauer Set, Eijkelkamp Soil & Water, Giesbeek, The Netherlands) and stored at -18°C. In September, additional soil samples were taken from the saturated sediment zone.

2.2.5 Radon (^{222}Rn) measurements

The geogenic gas ^{222}Rn is a commonly used natural tracer for groundwater influence in aquatic systems and is additionally known as a useful tool to trace the origins of CO_2 (Cook and Herczeg 2000; Megonigal et al. 2020). Therefore, ^{222}Rn concentrations and fluxes were measured with the RAD7 (RAD7 Radon Detector, DURRIDGE, Billerica, Massachusetts, USA) to determine the groundwater influence on CO_2 fluxes from dry river sediments. The measurements of the RAD7 are based on electrostatic collection of alpha-emitters with spectral analysis. Measuring with the "Normal" mode counts decays of both Polonium decay products of ^{222}Rn (^{218}Po, ^{214}Po). The counts are measured over an hour and averaged, with a standard deviation of one sigma. The measurement range lies between 4 – 750000 Bq m^{-3} with an accuracy of ± 5 %. Additionally, environmental factors may affect the precision by 2% (DURRIDGE 2021).

The ^{222}Rn concentration was measured in the groundwater, the distant groundwater and the river water. For that purpose, samples of ~ 300 ml were taken from the groundwater and the river and measured with the Wat250 mode. In Addition to that ^{222}Rn emissions from the soil were estimated with chamber measurements with the RAD7 over 3h, once per hour. Based on the assumption that groundwater is the main source of CO_2 and the fact that ^{222}Rn moves at the same mass flow as CO_2 (Megonigal et al. 2020), the same spatial dependences of CO_2 and ^{222}Rn fluxes were expected at the study site. For this reason, ^{222}Rn chamber measurements were performed simultaneously at two different positions, one with low and one with high CO_2 fluxes, which were determined in advance. To measure ^{222}Rn simultaneously two chambers of different sizes were used. Therefore, ^{222}Rn chamber flux measurements in Bq m^{-3} d^{-1} were corrected for different chamber volumes by multiplying with the volume [m^3] and dividing by the area [m^2] of the chamber, receiving results in Bq m^{-2} d^{-1}.

2.3 Analytical methods

2.3.1 Soil samples analysis

Soil samples were analyzed to determine soil moisture content, bulk density, and loss on ignition, along the measurement transect and at the sites of the automatic chambers. Therefore, a defined volume (10 ml) of soil sample was weighed and dried at 105 °C until constant weight, followed by combustion at 550°C. The sample weight was measured in between each step.
The bulk density (bd) of the sediment was estimated with the measured dry weight (m_{dry}) divided by the volume and is given in g cm^{-3}. The soil moisture content (θ) [vol%] was estimated by equation (1), where m_{fresh} is the weight of the fresh sample [g].

$$\theta = \frac{m_{fresh}\text{-}m_{dry}}{m_{dry}} \times bd \times 100 \quad (1)$$

Additionally, loss on ignition (LOI) [%] was calculated by equation (2), to estimate the organic matter content, where m_{com} is the sample weight after combustion at 550 °C [g].

$$LOI = \frac{m_{dry}\text{-}m_{com}}{m_{fresh}} \times 100 \quad (2)$$

2.3.2 Incubation experiments

Incubation experiments were set up to analyze the potential of microbial respiration from dry river sediments. For this purpose, fresh soil samples, taken along the transect were incubated in ~ 130 ml vials in replicates of four at 19.5 °C (while measured air temperature in the field varied between 10 to 27 °C, over the day). To determine the temperature dependence of the microbial respiration additional soil samples were taken for an additional incubation experiment. Therefore, soil samples were incubated at 4, 12, 19.5, 28 and 35 °C in replicates of four. With a Pressure-Lok® syringe (Pressure-Lok® glass syringe, Valco Instruments, Waterbury, Houston, USA) 4 to 5 gas samples were taken, over 2 to 3 days in regular intervals, from each incubated vial. The CO_2 and CH_4 concentrations in the gas samples were measured with the Gas Chromatograph (GC) (Gas Chromatograph System SRI 8610C, SRI Instruments Europe, Bad Honnef, Germany). The GC is equipped with a Flame Ionization Detector for hydrocarbons and a Methanizer which allows simultaneous measurement of CO_2 and CH_4, with an accuracy of < 5 %.

2.3.3 Groundwater and river water analysis

To analyze dissolved inorganic carbon (DIC) and dissolved organic carbon (DOC) in the groundwater and river water the water samples needed to be filtered with a glass microfiber filter, in advance. The DIC and DOC concentrations were analyzed based on high-temperature oxidation and NDIR-Detection (DIMATOC® 2000, DIMATEC Analysentechnik, Essen, Germany). The alkalinity of the water samples was determined by titration with HCl till a pH of 4.3 is reached (DMS Titrino, Metrohm, Herisau, Switzerland). To determine the concentration of the cations K^+, Na^+, Ca^{2+} and Mg^{2+} the water samples were filtered with a 0.45 µm syringe filter, acidified with HNO_3 and analyzed based on Spectroscopy with an ICP OES (Optima 7300 DV, Perkin Elmer, USA). The Anion concentrations of SO_4^{2-} and Cl^- were measured with ion chromatography (Dionex-ICS 6000, Thermo Fisher Scientific, Waltham, Massachusetts, USA). The samples were filtered with a 0.45 µm syringe filter, in advance. Isotope signatures of $\delta^{18}O$ and $\delta^{2}H$ were also measured, with the Triple Isotope Water Analyzer with Off-Axis Integrated Cavity Output Spectroscopy technique (TIWA-45-EP, Los Gatos Research, San Jose, California, USA). All stable isotope values are given in the common δ–notation described by (O'Leary 1981) and shown in equation (3).

$$\delta\,[‰] = \left(\frac{R_{sample}}{R_{standart}} - 1\right) \times 1000 \qquad (3)$$

2.3.4 Stable carbon isotope ($\delta^{13}C$) analysis

For the $\delta^{13}C$ analysis of the gas samples, partial pressure of CO_2 and CH_4 was analyzed in advance with the GC. Afterward, the $\delta^{13}CO_2$ signatures of the gas samples were analyzed with Cavity Ring-Down Spectroscopy (G2201-i CO_2 & CH_4 CRDS Analyzer, Picarro, Sant Clara, California, USA). For that the CO_2 partial pressure of the gas samples needed to be in the range of 380 to 2000 ppm. If the concentration was higher samples were diluted in a syringe with synthetic air from a gasbag.

To analyze $\delta^{13}C$ signatures of the organic matter, the sand and the organic matter in the soil samples needed to be separated. This was done by suspension and decantation with ultrapure water. Afterward, the samples were dried at 45 °C for 24 h. For the measurements, the dried and homogenized samples have been weighed in tin cartouches with a mass of 3.5 to 5 mg. The carbon and nitrogen content and $\delta^{13}C$ and $\delta^{15}N$ signatures were measured with the Element Analyzer and the downstream mass spectrometer (EA IsoLink™ IRMS System, Thermo Fisher Scientific, Waltham, Massachusetts, USA).

All $\delta^{13}C$ signatures are given in the common δ-notation described by (O'Leary 1981) and shown in equation (3).

2.4 Data processing

2.4.1 Fluxes and environmental variables

The gas fluxes were estimated based on linear regression and calculated according to equation (4), where $\frac{\Delta C}{\Delta t}$ is the slope of the change in concentration over time [µatm d^{-1}], V is the volume of the chamber [m^3], A is the sediment area that is covered by the chamber [m^2], T is the temperature [K] and R is the ideal gas constant = 8.314 l atm K^{-1} mol^{-1}.

$$F = \frac{\Delta C}{\Delta t} \times \frac{V}{R \times T \times A} \tag{4}$$

For the gas fluxes of the manual measurements, the change in concentration over time was visually checked for linearity in advance. Calculations were made with the R package glimmr (Keller 2020).

2.4.2 Hydrology

The hydraulic gradient (hg) was calculated based on equation (5), where $h1_{pot}$ and $h2_{pot}$ are the hydraulic head measurements [m] from two different piezometers and Δl is the length of the flow path [m].

$$hg = \frac{h2_{pot} - h1_{pot}}{\Delta l} \tag{5}$$

The hydraulic conductivity was calculated based on Hvorslev (1951). Therefore, the piezometer was filled with water and the water level was measured till the at-rest water level was reached. The change of water level over time was normalized based on equation (6), where t is time [s], H(t) is the measured change of water level over time [m s^{-1}], H_0 is the water level at t = 0 s, where the piezometer is completely filled with water and H_{min} is the at-rest water level.

$$H_{norm}(t) = \frac{H(t) - H_{min}}{H_0 - H_{min}} \tag{6}$$

The natural logarithm of $H_{norm}(t)$ is plotted against the time and a slope is fitted ($\ln(H_{norm}(t))$ vs. t). The horizontal hydraulic conductivity (K) [m s^{-1}] is calculated by

equation (7), where D is the diameter of the piezometer [m] (D = 0.027 m), m is the anisotropy ratio which is assumed to be 7, L is the length of the screen [m] (L = 0.1 m) and T_{lag} is defined by equation (8), with *expo* describing the exponent of the exponential slope fitted in advance.

$$K = \frac{D^2 \times ln\left(m \times {}^{L}\!/_{D} + \sqrt{1 + (m \times {}^{L}\!/_{D})^2}\right)}{8 \times L \times T_{lag}} \tag{7}$$

with

$$T_{lag} = \frac{1}{|expo| \times ln(0.37)} \tag{8}$$

2.4.3 Incubation experiment and temperature response

Incubation experiments were performed to estimate the potential microbial respiration of the sediment. The amount of CO_2 in each incubation vial was calculated based on the ideal gas law (Eq. 9), where n is the amount of CO_2 [µmol], p is the partial pressure of CO_2 [ppm], R is the ideal gas constant = 82.057 cm^3 atm mol^{-1} K^{-1} and T is the temperature [K]. Based on linear regression the production rate r [µmol g^{-1} d^{-1}] is calculated according to equation (10), where $\frac{\Delta n}{\Delta t}$ is the change of CO_2 in the vial over time [µmol d^{-1}] and m_{dry} is the dry weight of the sediment in the vial [g].

$$n = \frac{p \times V}{R \times T} \tag{9}$$

$$r = {}^{\frac{\Delta n}{\Delta t}}\!/_{m_{dry}} \tag{10}$$

Estimated production rates were summarized and tested with the Wilcoxon-sum-rank test to determine whether samples in August and September differentiate from each other.

With the assumption that production rates of microbial respiration are uniform over the unsaturated zone in the sediment, fluxes [mmol m^{-2} d^{-1}] were calculated by equation (11), where h_0 is the thickness of the unsaturated zone [m].

$$F = \frac{r}{1000} \times bd \times h_0 \tag{11}$$

The temperature response of biological processes can be described by the exponential Boltzman-Arrhenius model (Eq. 12). Where v is a process rate, r_0 a normalization constant, E_a the activation energy [eV], k the Boltzmann constant = 8.617×10^{-5} eV K^{-1}, and T is the temperature [K].

$$v = r_0 \times e^{\frac{-E_a}{k \times T}} \quad (12)$$

To evaluate the temperature response of the microbial respiration in the sediment Q10 temperature coefficient (Eq. 13) and the activation energy (E_a) was used (Dell et al. 2011). Therefore, the natural logarithm of the production rate (ln(r)) was plotted against the reciprocal of k × T (see Appendix Fig. A1 & A2). The slope of these so-called Arrhenius plots was used to calculate the activation energy as described in Gillooly et al. (2001).

$$Q10 = \left(\frac{r_2}{r_1}\right)^{\left(\frac{10}{T_2 - T_1}\right)} \quad (13)$$

2.4.4 Chemical equilibrium of groundwater and river water

With the measured concentrations of ions, DIC, pH, alkalinity and temperature, the saturation index (SI) of the measured species in the groundwater was calculated, to estimate the possibility of $CaCO_3$ precipitation. Calculations are based on equation (14) where IAP is the ion activity product [mol^2 L^{-2}] and K is the solubility product [mol^2 L^{-2}]. For the calculations, the software Visual MINTEQ (Gustafsson 2020) was used.

$$SI = log\left(\frac{IAP}{K}\right) \quad (14)$$

The headspace equilibration is a common method based on Henry's law, where gas concentrations of CO_2 and CH_4 in the water are calculated from partial pressures in the headspace (UNESCO/IHA 2010). The concentration of the gas in the water samples is calculated according to equation (15), where c is the concentration [µmol L^{-1}], n_{tot} is the amount of CO_2 [µmol] and V_w is the volume of the water sample [L].

$$c = \frac{n_{tot}}{V_w} \quad (15)$$

with

$$n_{tot} = n_g + n_w - n_h \quad (16)$$

Equation (16) was used to calculate n_{tot}, where n_g is the amount of CO_2 in the gas space, n_w is the amount of CO_2 in the water and n_h is the background amount of CO_2 that was introduced by adding the headspace gas.

To calculate n_g [µmol], equation (9) was applied. The same equation (Eq. 9) was used for n_h with the difference that the measured CO_2 concentration of the headspace gas was used. Further, n_w (Eq. 17) was calculated with the help of the Bunsen coefficient (α) (Eq. 18), where H is the Henry coefficient for the equilibration temperature [mol L^{-1} atm^{-1}] provided by Sander (2015). All calculations are based on UNESCO/IHA (2010).

$$n_w = \frac{p \times \alpha \times V_w}{R \times T} \quad (17)$$

with

$$\alpha = H \times R \times T \quad (18)$$

Considering that CO_2 is in equilibrium with other carbonate species in the water, the application of Henry's law is not sufficient to estimate the CO_2 concentrations. Therefore, a correction of the CO_2 concentration as described in Koschorreck et al. (2020) was applied.

Just as the potential respiration was estimated, a proxy for the potential of CO_2 degassing from the groundwater is provided by an estimation of the potential groundwater evaporation. This is based on the assumption of simultaneous transport of water and gas through the unsaturated zone. Because surface run-off was not observed, and soil moisture was considerably low, where high CO_2 fluxes were measured, complete evaporation of the amount of water that reaches the sediment-atmosphere interphase was assumed. To estimate if the outgassing CO_2 from the groundwater could cover the measured fluxes, the measured DIC was used to calculate the amount of groundwater that would need to reach the sediment-atmosphere interphase. Further, this leads to the question, how much groundwater would need to evaporate to cover the measured (minimum, maximum and average) CO_2 fluxes. Therefore, it was assumed that dissolved CO_2 in groundwater is the only CO_2 source of the CO_2 emissions at the study site. For further calculations, it needs to be considered that CO_2 is part of the carbonate equilibrium

and is therefore affecting other carbonate species during the process of outgassing. Each molecule of CO_2 outgassing causes one molecule of carbonate precipitation, to re-equilibrate with the atmosphere (Eq. 19) (Sigg and Stumm 2016). Thus, it was assumed that half of the DIC is outgassing as CO_2 and the other half is precipitating as $CaCO_3$.

$$2 \times HCO_3^- + Ca^{2+} = CO_2\,(g) + CaCO_3\,(s) + H_2O \quad (19)$$

Based on that, the potential groundwater evaporation E_{GW} [L m^{-2} d^{-1}] is calculated by the equation (20), with the CO_2 flux (F) [mgC m^{-2} d^{-1}] and DIC [mg L^{-1}].

$$E_{GW} = \frac{F}{DIC/_2} \quad (20)$$

2.4.5 Stable carbon isotopes ($\delta^{13}C$)

The $\delta^{13}CO_2$ signatures [‰] from the discrete gas samples were plotted against the reciprocal of the CO_2 concentration [1 ppm^{-1}] and a linear regression model was fitted (see Appendix Fig. A3). These so-called Keeling plots were visually checked for linearity. The isotopic signal of the sediment flux can be calculated as the y-intercept of the linear regression and is based on the steady-state assumption and that both source and background $\delta^{13}CO_2$ signatures remain constant over the measurement period (Keeling 1958). Additionally, the isotopic signal of the sediment flux was corrected (F_{cor}) for the theoretical diffusive fractionation of –4.4 ‰ as described in Cerling et al. (1991). All $\delta^{13}C$ isotope flux and the endmembers signatures were summarized, respectively and tested with Kruskal-Wallice test and Dunn's posthoc test whether samples originate from the sample distribution and if groups differ significantly from each other.

2.5 Data analysis

2.5.1 Fluxes and environmental variables

Firstly, the CO_2 flux data sets from manual and automatic measurements were visually checked for normality with the Q-Q-plot. The CO_2 fluxes from the manual measurements were summarized by date and tested with univariate ANOVA and posthoc paired t-test whether samples originate from the sample distribution and if groups differ significantly from each other. Additionally, the data were summarized by distance to the river and tested with a one-sample t-test to determine if measured fluxes differentiate significantly from zero.

The spatial and temporal patterns of the measured CO_2 fluxes and environmental variables at the study site were analyzed to identify relations between the environmental variables and the CO_2 flux. The Spearman rank correlation was used to determine if relationships can be found between environmental variables and the CO_2 flux, and to identify the strength and direction of these relations (Leyer and Wesche 2007). Additionally, representative periods and single days were selected from automatic measurements to analyze patterns, hidden by the temporal variability of the data. Therefore, cross-correlation was applied to identify time lags. The measured environmental variables of soil temperature, soil moisture, thickness of the unsaturated zone, organic matter content and precipitation were used for correlation analysis. The precipitation data was provided by the DWD weather station in Magdeburg (Deutscher Wetterdienst 2020), ~ 15 km linear distance to the study site and was accessible through the R package rdwd (Boessenkool 2020). Moreover, water level data was used to determine a proxy of the unsaturated zone if not measured and was available from the LHW Sachsen-Anhalt (LHW 2020), measured at 327 km, ~ 13 km downstream of the study side. The additional data was averaged over 1 hour. The soil moisture data of the automatic measurements showed high heterogeneity with a high error [%] compared to the analysis of the sediment samples (Fig. 4), suggesting that the data does not display the real heterogeneity at the study site but rather showing differences in calibration. Therefore, the soil moisture data from the automatic measurements were excluded from further analysis.

To apply simple linear regression models and linear mixed models (lmm) assumptions of normality and homoscedasticity were visually checked with diagnostic plots, including residuals vs. fitted and Q-Q-plot. Lmm were applied to predict the influence of the environmental variables on the CO_2 flux at the study site, for variables where a linear relationship with the CO_2 flux was presumed.

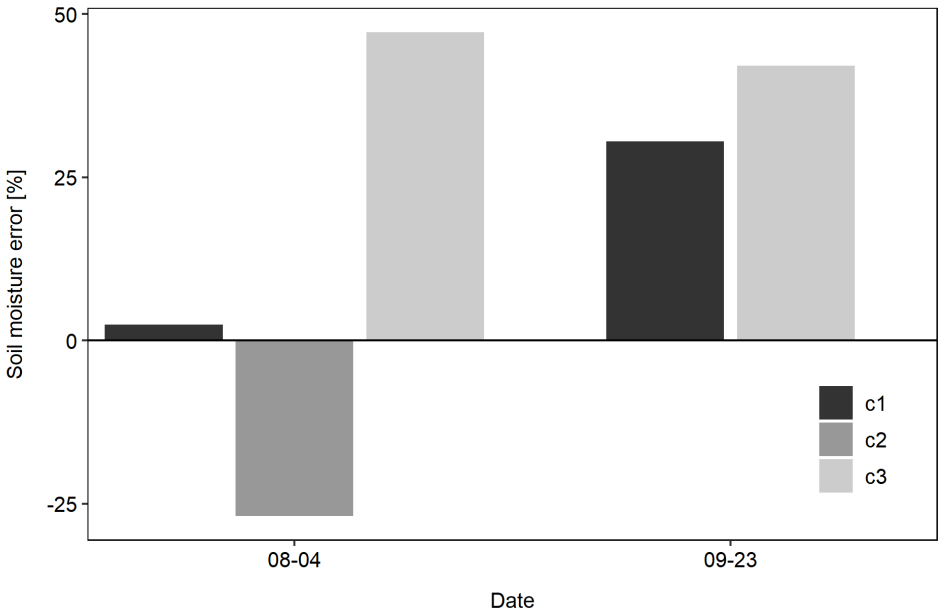

Figure 4: Estimated error of soil moisture from automatic measurements compared to soil moisture determined in the laboratory. The different shades of grey indicate the three different automatic chambers (C1, C2 and C3) that were used for measurements.

3 Results

3.1 Site characteristics

3.1.1 Fluxes from dry river sediments

The CO_2 fluxes measured from desiccated sediment at the river Elbe ranged from −120 to 1135 mmol m^{-2} d^{-1} with a mean (± SD) of 148 (± 155) mmol m^{-2} d^{-1}. It was observed that the CO_2 fluxes from the manual measurements were lower and covered a smaller range than the CO_2 fluxes from the automatic measurements (Tab. 2). Differences between dark and light CO_2 flux measurements appeared only occasionally and in a negligible range. Furthermore, CH_4 fluxes were rarely measured with a comparable low mean of 0.4 (± 0.8) (Tab. 1), while fluxes of N_2O were not observed, because N_2O concentrations were under the detection limit.

Table 2: Summary of measured CO_2 and CH_4 fluxes [mmol m^{-2} d^{-1}], from manual and automatic measurements at the study site.

Measurements	Gas	n	Min.	Max.	Mean	SD	Median
All	CO_2	3224	-120	1135	148	155	98
Manual	CO_2	96	-28	219	82	63	87
Manual	CH_4	22	-0.5	3.4	0.4	0.8	0.3
Automatic	CO_2	3128	-120	1135	149	155	98

In general, the CO_2 fluxes showed temporal and spatial heterogeneity for both measurement types. In Figure 5, a diurnal pattern of the CO_2 fluxes and high temporal variability between the measurement days could be observed during the automatic measurements. Additionally, generally higher CO_2 fluxes were noticeable for the automatic measurements, when chambers were positioned at a greater distance to the river (e.g. position 85) indicating spatial differences. Moreover, negative fluxes were observed over all positions of the automatic measurements (Fig. 5).

Temporal variability between different measurement days was also observed for the manual measurements. However, measured data from each measurement day did not significantly differ from each other (Fig. 6) (ANOVA: Df = 5, F = 3.4, p = 0.006). Furthermore, a spatial pattern of increased fluxes with increasing distance to the river was observable for the manual measurements (Fig. 6). The manual measured CO_2 fluxes directly at the river up to a one-meter distance to the river did not significantly differ from zero. From a two-meter distance to the river, the CO_2 fluxes increased visible and differed significantly from zero. Additionally, negative fluxes were observed, primarily in < 3 m distance to the river (Fig. 6).

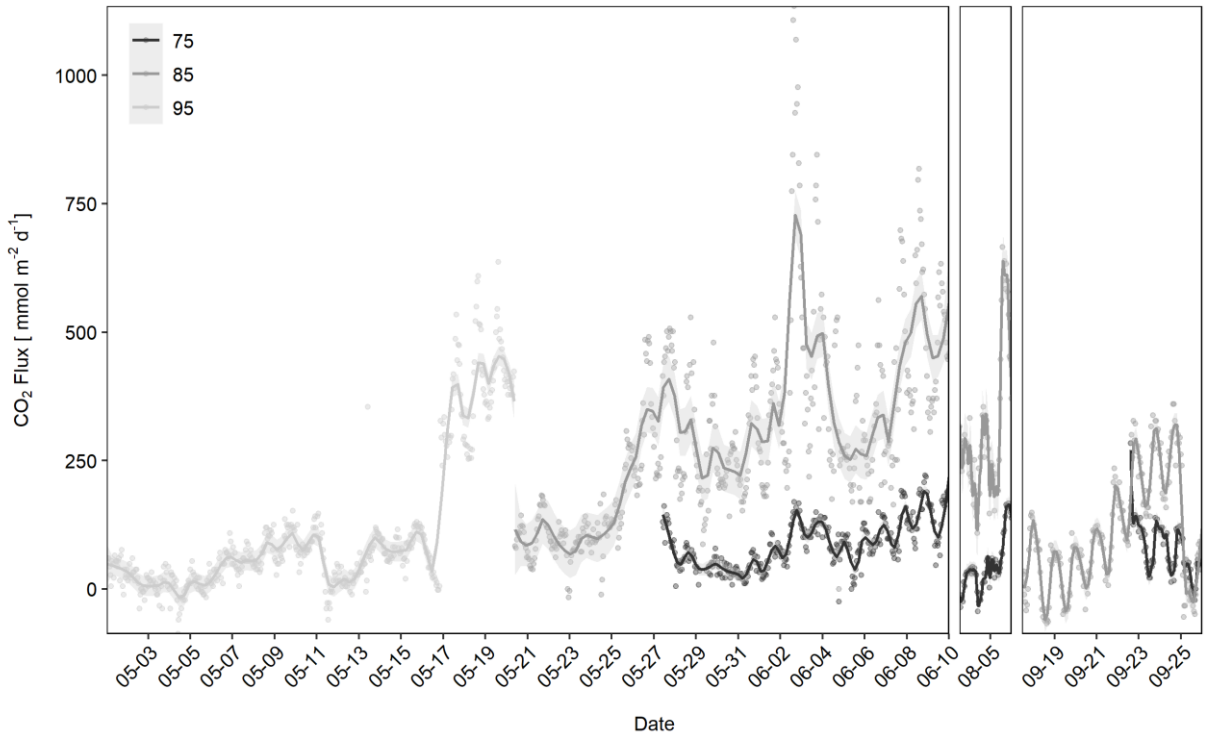

Figure 5: The CO_2 fluxes from automatic measurements. The color indicates the position of the automatic chamber over gauge zero [cm]. The measured fluxes are visualized by points. The line represents the smoothing of the data with SD. It should be noted that only in May the automatic chambers were placed 95 cm over gauge zero.

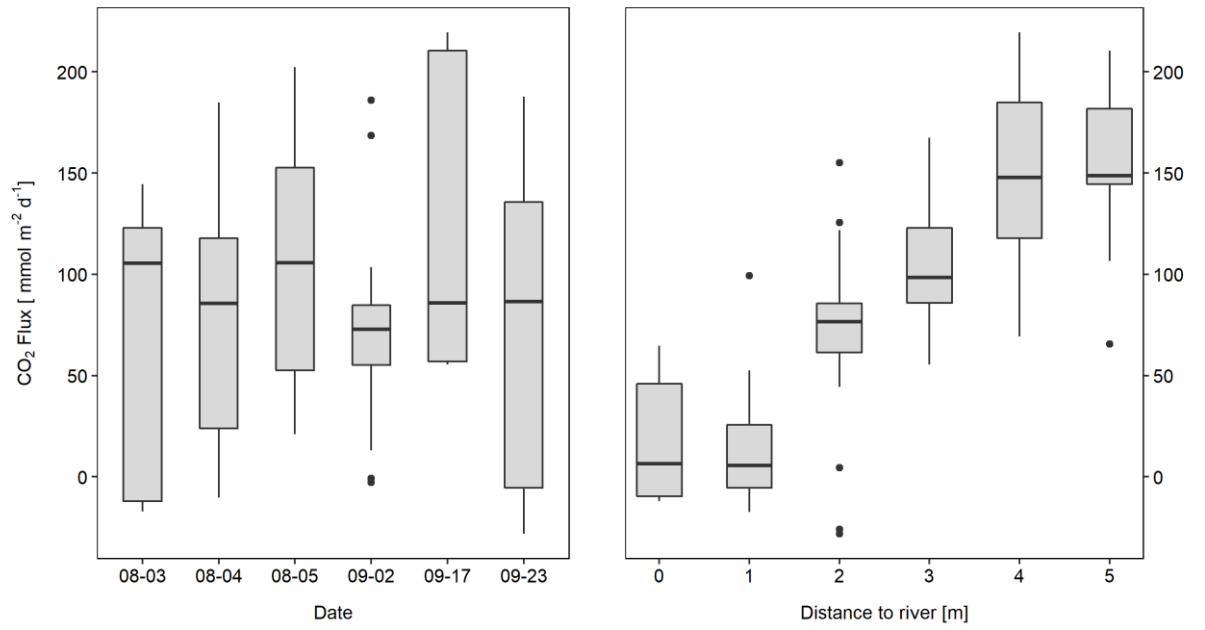

Figure 6: The CO_2 fluxes from manual measurements. On the left, CO_2 fluxes are summarized by date and tested with univariate ANOVA with a paired t-posthoc test. On the right, CO_2 fluxes are summarized by distance to the river and tested with a one-sample t-test, to determine if fluxes significantly differ from zero.

3.1.2 Hydrology

The hydraulic conductivity at the study site was high, varying between 9.59×10^{-5} and 4.87×10^{-4} m s^{-1} in a depth between 50 – 90 cm, which can be considered as a typical range for middle or silty sand. A hydraulic gradient was almost not observable. Only on the 2nd of September, a gradient towards the river was noticeable (hg = 0.08). The measured $\delta^{18}O$ and $\delta^{2}H$ signatures (see Appendix Tab. A1) of the groundwater did not show a significant difference between the piezometer nor between groundwater and surface water ($\delta^{2}H$ = –57 (± 1.0) ‰, $\delta^{18}O$ = –7.8 (± 0.1) ‰). Nevertheless, stable water isotope ratios at the study site were less negative compared to the far distant groundwater wells ($\delta^{2}H$ = –62 (± 2.6) ‰, $\delta^{18}O$ = –8.7 (± 0.4) ‰).

3.2 The main source of CO_2 emissions

3.2.1 Potential of microbial respiration

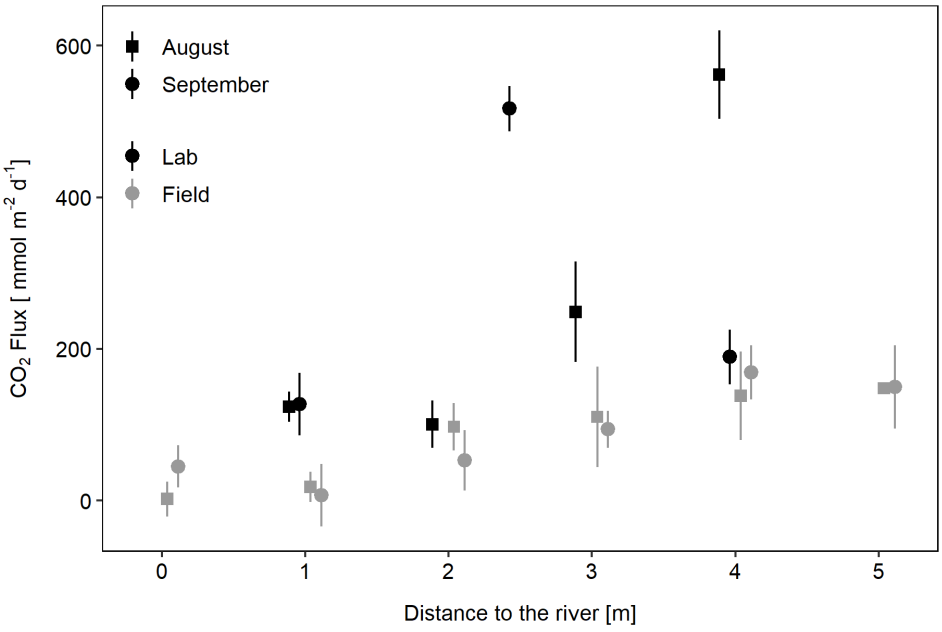

Figure 7: The calculated CO_2 fluxes from incubation experiments (black) compare to CO_2 fluxes measured in the field (grey), in August (square) and in September (circle). It should be noted that fluxes calculated from the incubation experiment are based on the assumption that the production of CO_2 is uniform over the unsaturated zone.

The potential CO_2 emissions from microbial respiration were estimated with incubation experiments in August and September to determine, whether microbial respiration from the sediment can cover the measured CO_2 fluxes in the field.

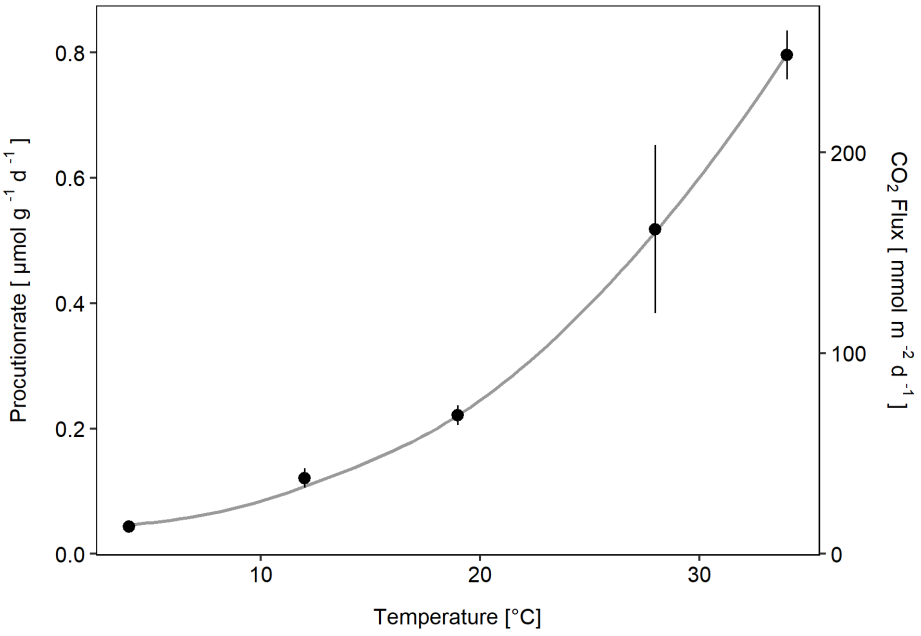

Figure 8: The temperature response of dry river sediment from Incubation experiment, incubated at 4, 12, 19, 28 and 34 °C. The left axis shows the production rate, while the right axis shows the CO_2 fluxes. It should be noted that calculations of CO_2 production rates and fluxes are based on the assumption that the production of CO_2 is uniform over the unsaturated zone.

The production rate of the incubation was higher in September with 0.9 (± 0.45) µmol g^{-1} d^{-1} than in August with 0.64 (± 0.22) µmol g^{-1} d^{-1} but did not significantly differ from each other (Wilcoxon rank-sum test: W = 66, p-value = 0.171).

In general, the estimated ex-situ fluxes (Lab) covered the measured in-situ fluxes (Field) and in some instances were even a magnitude higher (Fig. 7). However, it should be noted that air temperature during the field measurements covered a wider range than the incubation temperature, at 19.5 °C and that the flux calculations from the incubation experiments are based on the assumption that production of CO_2 is uniform over the unsaturated zone.

Furthermore, an additional incubation experiment revealed a recognizable increase of the CO_2 production rate, with increasing temperature. The observed temperature response of the CO_2 production in the river sediment appeared to be exponential (Fig. 8). Based on this, the Q10 value of 2.5 was estimated over a temperature range of 19 to 28 °C, a range also observed in the field. The activation energy from the incubation experiment was additionally estimated with a value of 0.7 eV.

3.2.2 Potential of groundwater evaporation

To estimate whether degassing CO_2 from the groundwater has an influence on the CO_2 emissions at the study site, potential evaporation rates of groundwater that would be necessary to cover the measured CO_2 fluxes were estimated. The DIC concentrations in the groundwater

ranged between 23.4 to 70.4 mg L^{-1} and were slightly higher in September (see Appendix Tab. A3). The groundwater evaporation that would be needed to cover the minimum, average and maximum CO_2 flux, measured in August and September, was estimated respectively and presented in Table 3. Due to differences in DIC content, estimated evaporation rates differed between August and September. Generally, it can be observed that compared to potential evaporation rates (E_{pot}) from 2010 (LAU 2021), potential groundwater evaporation rates (E_{GW}) that would be needed to cover maximum CO_2 fluxes at the study site are high (Tab. 3).

Table 3: The estimates of potential groundwater evaporation (E_{GW}) to cover the minimum (Min.), average (Mean) and maximum (Max.) CO_2 fluxes at the study site. For comparability, the potential evaporation rates (E_{pot}) from Magdeburg in 2010 provided by LAU (2021) are presented.

Date	Min. E_{GW} [L m^{-2} d^{-1}]	Mean E_{GW} [L m^{-2} d^{-1}]	Max. E_{GW} [L m^{-2} d^{-1}]	E_{pot} [L m^{-2} d^{-1}]
2020-08-04	0	42	89	3.4
2020-09-23	2	28	64	2.3

3.2.3 Stable carbon isotope signatures ($\delta^{13}C$)

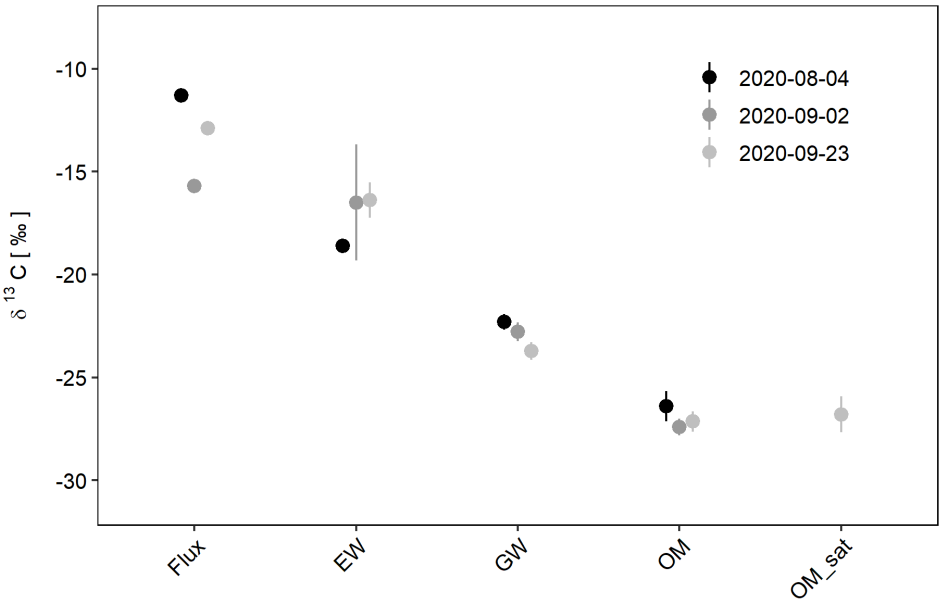

Figure 9: The mean (± SD) $\delta^{13}C$ signatures at the study site for each measurement day. Showing the CO_2 flux signatures (Flux), the $\delta^{13}DIC$ signatures from the river Elbe (EW), the $\delta^{13}DIC$ signatures from the groundwater (GW) and the $\delta^{13}C$ signatures from the organic matter of the saturated (OM_sat) and unsaturated (OM) zone.

The results of the Keeling plot approach showed $\delta^{13}C$ signatures of the diffusive CO_2 flux from dry river sediments (Flux) of −11.3 ‰ in August, −15.7 ‰ and −12.9 ‰ in September (Fig. 9). Compared to the measured endmembers, the CO_2 flux $\delta^{13}C$ signatures estimated from the Keeling plots were the heaviest at the study site. Correcting the CO_2 flux $\delta^{13}C$ signatures by the theoretical diffusive fractionation of −4.4 ‰ (Flux_cor), resulted in even heavier $\delta^{13}C$ signatures (Fig. 9). The $\delta^{13}C$ signatures of the river water DIC were likewise comparable heavy, with −18.6 ‰ in August, −16.5 ‰ and −16.4 ‰ in September (Fig. 9). Moreover, $\delta^{13}DIC$ signatures of the groundwater were similar between the piezometers, regardless of the increasing distance to the river, varying around a mean (± SD) of – 22.9 ‰ (± 0.8) and did not significantly differ from the $\delta^{13}DIC$ signatures of the river water (Dunn's posthoc test: p = 1.00). The sediment organic matter $\delta^{13}C$ signatures were the lightest endmembers at the study site with a mean (± SD) of −26.9 ‰ (± 0.8). Thereby, differences between saturated and unsaturated sediment were not significant (Fig. 10) (Dunn's posthoc test: p = 1.00). Generally, the Kruskal-Wallice test with Dunn's posthoc test showed that only sediment organic matter $\delta^{13}C$ signatures differed significantly from the $\delta^{13}CO_2$ flux signatures (Fig. 10) (see Appendix Tab. A5) (Kruskal-Wallice test: Chi-squared = 57.29, df = 6, p-value = 1.60×10^{-5}).

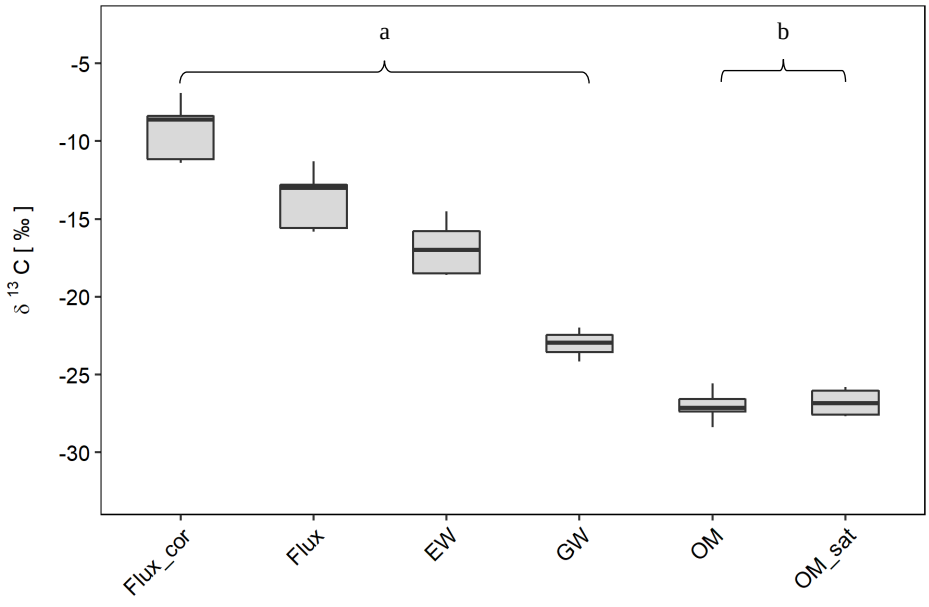

Figure 10: The $\delta^{13}C$ signatures at the study site, all measurements summarized by boxplots. Showing the CO_2 flux signatures corrected for diffusive fractionation (Flux_cor), the CO_2 flux signatures (Flux), the $\delta^{13}DIC$ signatures from the river Elbe (EW), the $\delta^{13}DIC$ signatures from the groundwater (GW), and the $\delta^{13}C$ signatures from the organic matter of the saturated (OM_sat) and unsaturated (OM) zone. The letters indicate results from the Kruscal-Wallice test with Dunn's posthoc test, showing that only OM significantly differs from the $\delta^{13}CO_2$ flux signatures.

3.2.4 Radon (^{222}Rn)

The ^{222}Rn concentration in the groundwater was 6090 (± 418) Bq m^{-3} in August and 6650 (± 436) Bq m^{-3} in September. Although, the more distant groundwater in the flood plain covered with 8470 (± 491) Bq m^{-3} and 5040 (± 387) Bq m^{-3} a wider range, the concentrations were similarly high compared to the ^{222}Rn concentrations of the groundwater at the study site. The ^{222}Rn concentrations in the river were much lower with 327(± 109) Bq m^{-3} in August and 532 (± 135) Bq m^{-3} in September. The chamber measurements of ^{222}Rn indicated higher ^{222}Rn emissions from the sediment in September compared to emissions in August (Tab. 4). In August the measured ^{222}Rn fluxes were similar, regardless of the distance to the river or the CO_2 flux. In September however, it was observed that the ^{222}Rn flux was higher with a greater distance to the river, where high CO_2 fluxes were measured (Tab. 4).

Table 4: The ^{222}Rn fluxes at the study site with distance to the river, in August and September. For comparison, the mean (± SD) CO_2 fluxes are also provided.

Date	Distance to river [m]	^{222}Rn flux [Bq m^{-2} d^{-1}]	CO_2 flux [mmol m^{-2} d^{-1}]
2020-08-05	1	64.51	18 (± 20)
2020-08-05	3	62.92	110 (± 31)
2020-09-23	1	174.30	7 (± 41)
2020-09-23	4	205.42	169 (± 36)

3.3 Influence of environmental variables on the CO_2 flux

3.3.1 Automatic measurements

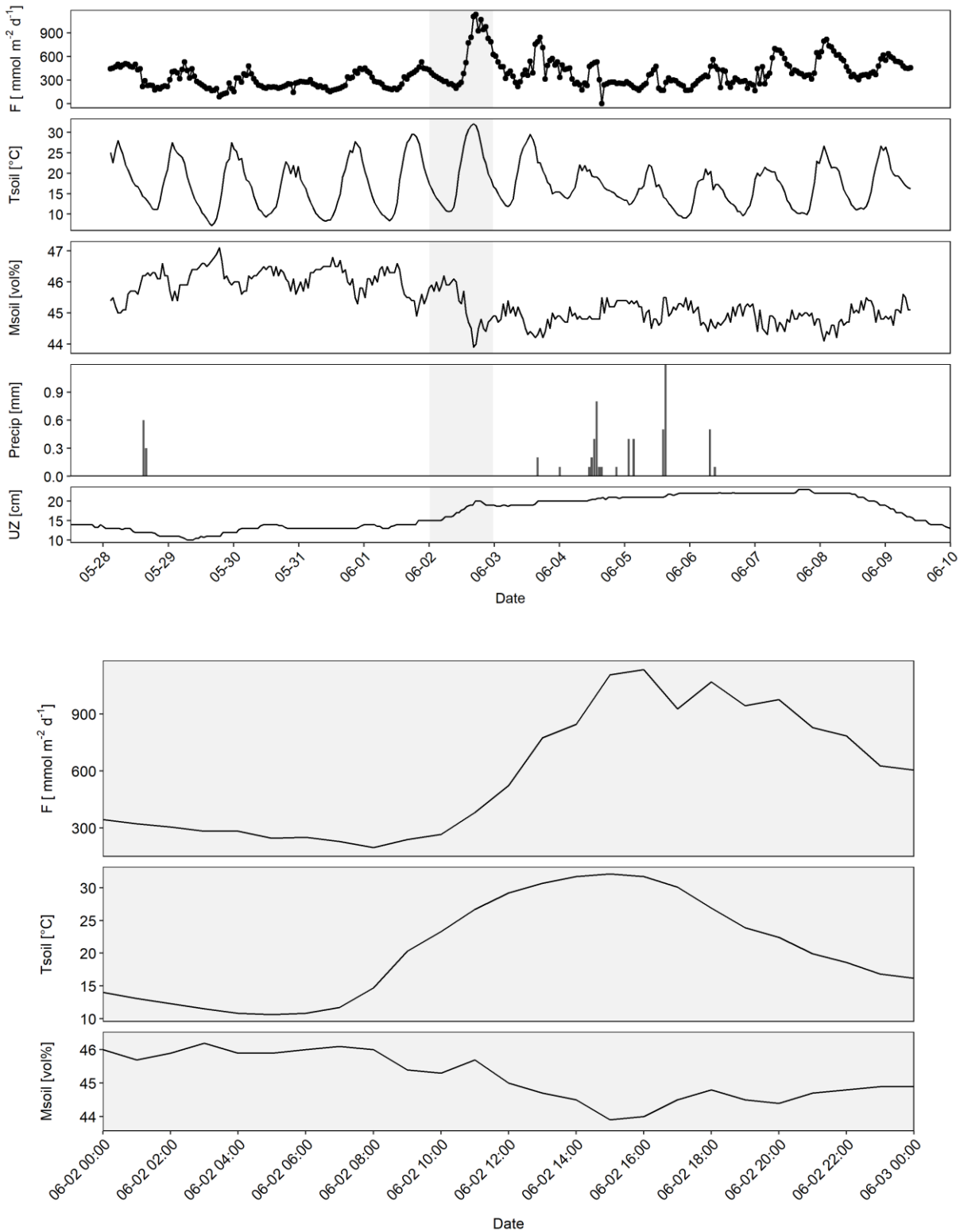

Figure 11: The CO_2 fluxes (F) and the environmental variables: Soil temperature (Tsoil), soil moisture (Msoil), Precipitation (Precip) and thickness of the unsaturated zone (UZ) from automatic measurements. The CO_2 fluxes and environmental variables during a representative period in June (top) with the 2nd of June highlighted in grey. The CO_2 flux and environmental variables with observed diurnal pattern, on the 2nd of June (bottom).

During the automatic measurements, the measured soil temperature and soil moisture showed a diurnal pattern over the measurement period, similar to the CO_2 fluxes. While temperature and CO_2 flux amplitudes were occasionally quite high, diurnal changes of soil moisture were usually in a range of 0 – 3 vol%, if no heavy precipitation event occurred. It was observed that CO_2 fluxes usually reached their maximum when soil moisture was at its daily minimum and soil temperature at its daily maximum. Recurrently, a slight temporal offset of this pattern was observable (Fig. 11). Moreover, data of soil moisture, temperature and the CO_2 fluxes showed irregularities of the diurnal pattern, especially during heavy events of precipitation. During and after precipitation the amplitudes of soil moisture and temperature were smaller, and an increase of soil moisture was observed, while soil temperature decreased. A decrease of the CO_2 flux was also noticeable, along with less pronounced daily amplitudes (Fig. 11). Not only precipitation but also the unsaturated zone seemed to influence soil moisture and the CO_2 flux, even though a diurnal pattern was not observed (Fig. 11 & Tab. 5). However, changes of the unsaturated zone were in a comparatively small range and cannot explain the diurnal pattern of CO_2 fluxes.

Although, all these relationships were observed variability of the automatically measured data was comparable high, resulting in weak relationships between flux and environmental variables (Tab. 5). However, it can be observed that diurnal environmental variables like soil moisture and temperature shape the diurnal pattern of the CO_2 emissions (Fig. 11). Indeed, patterns became clearer when looking at days separately. While soil moisture showed occasionally a negative linear relationship with the CO_2 flux, it should be considered that the soil moisture data from automatic measurements strongly differed from the reference soil moisture determined in the laboratory (Fig. 4 & see Appendix Fig. A10). Changes in the thickness of the unsaturated zone were in a small range and showed no consistent trend, when looking at the days separately, even though the correlation with the flux was comparable high (Tab. 5 & see Appendix Fig. A9).

Table 5: The Spearman correlation coefficients of automatically measured data, with the CO_2 fluxes (F) and the environmental variables: Soil temperature (Tsoil), soil moisture (Msoil), precipitation (Precip) and thickness of the unsaturated zone (UZ). The * indicates the significance ($p < 0.05$) of the correlation.

	F	Msoil	Tsoil	UZ	Precip
F	1				
Msoil	-0.19 *	1			
Tsoil	0.19 *	0.01	1		
UZ	0.31 *	-0.34 *	-0.15 *	1	
Precip	-0.12 *	0.02	-0.03	0.08 *	1

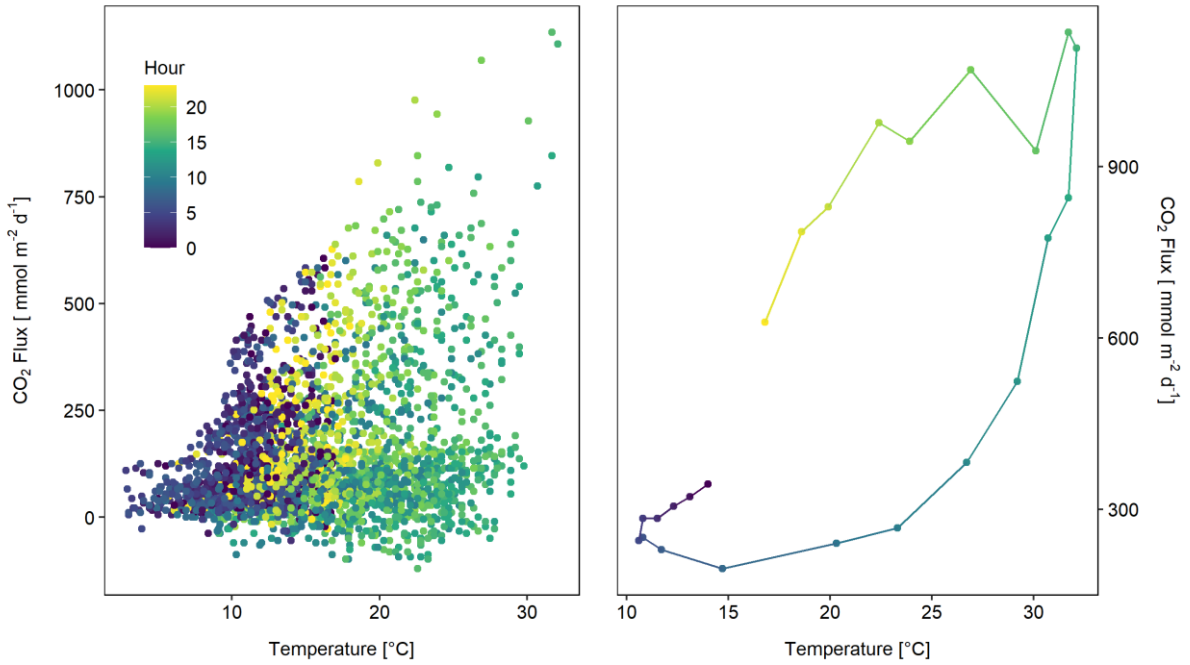

Figure 12: The temperature response of CO_2 fluxes over the measurement period (left) and on the 2nd of June (right). The colors represent the hour of the day.

The soil temperature however seemed to influence the CO_2 flux and a consistent pattern was observed (Fig. 12 & see Appendix Fig. A7 & A8). Having a closer look at a daily course of the relationship between temperature and CO_2 flux revealed an exponential increase of the CO_2 flux with increasing temperature. However, cooling during the night did not seem to decrease CO_2 flux exponentially, which leads to an observable hysteresis over the day (Fig. 12). This pattern was observed during several days over the measurement period, in June and August when production rates were comparable high (see Appendix Fig. A7 & A8). Occasionally, time lags up to 3 h were observed between CO_2 flux and soil temperature. Supporting the general observation of temperature response of the CO_2 fluxes, the incubation experiment in the laboratory revealed a comparable exponential increase of the CO_2 production rate from the river sediments with increasing temperature (Fig. 8 & Fig. 12). Additionally, the temperature response was shown by the Q10 value which lies at 2.5 over the temperature range of 19 – 28 °C based on the data from the incubation experiments, and at 3.1 over a comparable temperature range of 20 – 30 °C based on the automatic measurements. While Q10 values differ slightly, the activation energy estimated from automatic measurements on June 2nd was with 0.7 eV identical to the calculated activation energy from the incubation experiment (see section 3.2.1).

3.3.2 Manual measurements

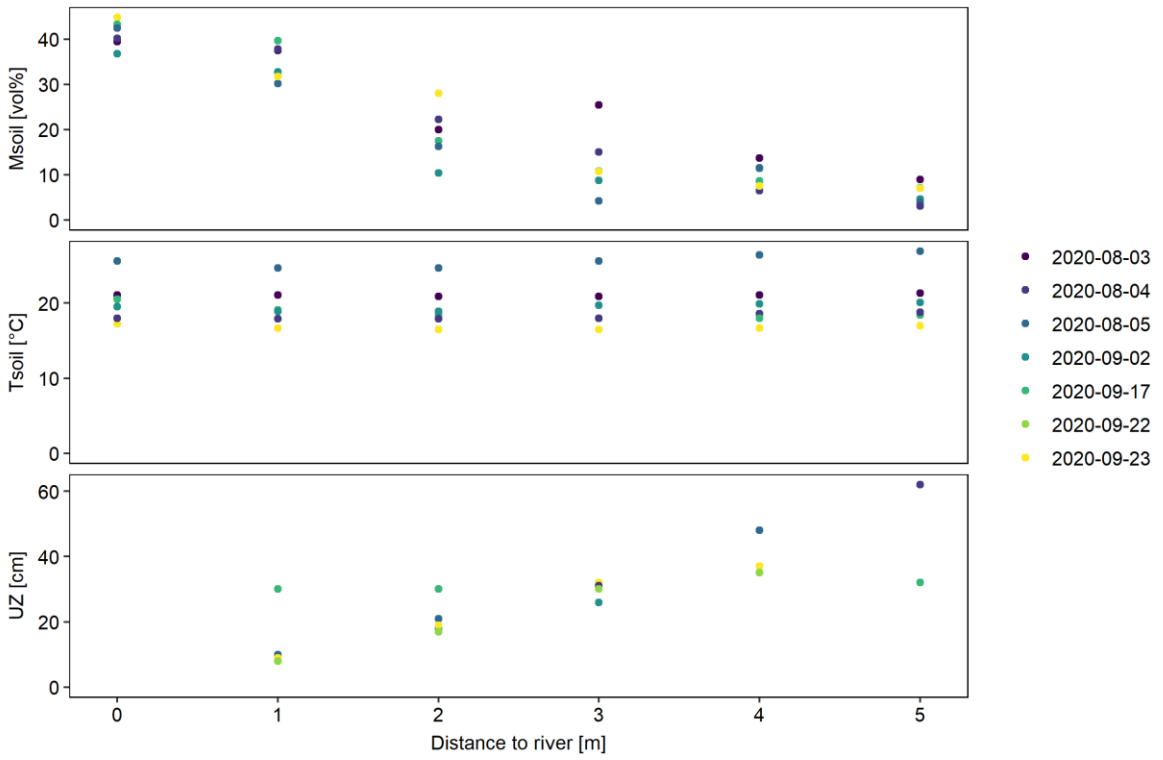

Figure 13: The environmental variables, soil moisture (Msoil), soil temperature (Tsoil) and thickness of the unsaturated zone (UZ) from the manual measurements, with distance to the river. The colors represent different measurement days.

Table 6: The results of soil moisture (θ), loss on ignition (LOI) and bulk density (bd) from soil sample analysis. The soil samples were taken in August and September (Date) at the sites of the automatic measurements and the manual measurements (Measurement). For the manual measurements, the soil samples were taken at different distances to the river.

Date	Measurement	Distance to river [m]	θ [vol%]	LOI [%]	bd [g cm^{-3}]
2020-08-04	manual	1	30	0.78	1.68
2020-08-04	manual	2	13	0.39	1.37
2020-08-04	manual	3	25	1.11	1.35
2020-08-04	manual	4	13	0.94	1.37
2020-08-04	automatic	-	43	6.56	1.40
2020-09-23	manual	1	29	0.85	1.46
2020-09-23	manual	2,5	26	0.97	1.43
2020-09-23	manual	4	9	0.52	1.36
2020-09-23	automatic	-	41	6.07	1.08

During manual measurements, no diurnal pattern was observed due to the discrete nature of the measurements, repeated maximal two or three times over a measurement day. Additionally, manual measurements took place along a transect. For this reason, the manually measured data rather covered the spatial variability than the temporal variability. The changes of soil temperature during manual measurements were compared to automatic measurements small over a measurement day and rather differed between the measurements (Fig. 13). Therefore, the correlation of temperature with the CO_2 flux was low and no relation between temperature and CO_2 flux was observable (Tab. 7). The organic matter content, described by the LOI, was generally low and a pronounced pattern of changes in organic matter with space or time was not observed, nor a relation between CO_2 flux and LOI (Tab. 6 & Tab. 7). The same applied to bulk density (Tab. 6).

Compared to the automatic measurements, the manually measured data of soil moisture were in a comparable range as the soil moisture content estimated in the laboratory (Tab. 6 & Fig. 13). Additionally, changes in the thickness of the unsaturated zone were more pronounced during manual measurements. The measured environmental variables of soil moisture and thickness of the unsaturated zone, and the CO_2 flux showed a similar pattern over all measurements. The soil moisture was decreasing linearly with the distance to the river, while the thickness of the unsaturated zone was increasing linearly with distance to the river along the hillslope at the study site (Fig. 13). Hence, high correlations were observed between soil moisture, the thickness of the unsaturated zone and the CO_2 flux, possibly indicating a causal relation (Fig. 14 & Tab. 7). Furthermore, it was observed that the relationship between the CO_2 fluxes and the environmental variables soil moisture and thickness of the unsaturated zone was linear, for the manual measurements (Fig. 14). Hence, linear mixed models (lmm) were applied to achieve improved prediction of the CO_2 flux.

Table 7: The Spearman correlation coefficients of manually measured data, with the CO_2 fluxes (F) and the environmental variables: Soil temperature (Tsoil), soil moisture (Msoil), thickness of the unsaturated zone (UZ) and loss on ignition (LOI). The * indicates the significance ($p < 0.05$) of the correlation.

	F	Msoil	Tsoil	UZ	LOI
F	1				
Msoil	-0.74 *	1			
Tsoil	0.18	-0.10	1		
UZ	0.79 *	-0.71 *	0.17	1	
LOI	0.09	-0.32	0.57 *	0.26	1

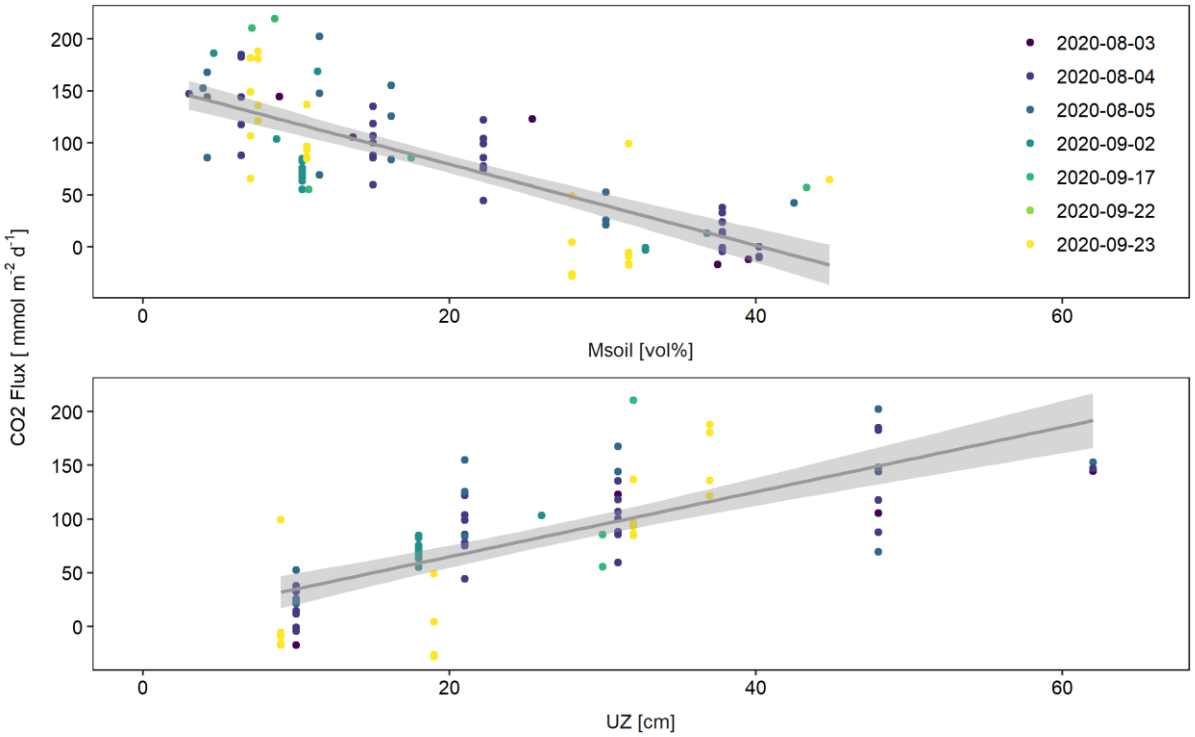

Figure 14: Relationship between CO_2 fluxes and the environmental variables soil moisture (Msoil) and thickness of the unsaturated zone (UZ) from manual measurements over the measurement period. The linear model (grey line) of CO_2 fluxes and environmental variables is presented with SD.

Including time as a random effect, resulted in a comparable small improvement of the model, indicating low temporal variability of the manually measured data (Tab. 8). Nevertheless, it could be shown that moisture and thickness of the unsaturated zone were reasonably good predictors for the CO_2 flux at the study site (Tab. 8 & Fig. 14). Assuming that CO_2 production is uniform over the unsaturated zone, the model suggested that the CO_2 flux increased by ~3 (± 0.5) mmol m^{-2} d^{-1} per one-centimeter increase of the unsaturated zone, with an intercept at ~7.5 (± 16) mmol m^{-2} d^{-1} describing the CO_2 flux, where the thickness unsaturated zone equals zero.

Table 8: The results from lmm with the measurement date as a random effect. The explained variability is described by R^2 marginal for the fixed effects only and by R^2 conditional describing the variability including fixed and random effects. The lmm were fitted for the environmental variables (Fixed), where a linear relations ship was presumed.

Measurement	Fixed	Random	Intercept (± SD)	Slope (± SD)	R^2 marginal	R^2 conditional
manual	UZ	Date	7.5 (16)	3 (0.5)	0.52	0.57
manual	Msoil	Date	161.2 (9.2)	-4 (0.3)	0.59	0.64

4 Discussion

The measured CO_2 emissions from dry sediment at the river Elbe (mean (± SD) = 148 (± 155) mmol m^{-2} d^{-1}, median = 98 mmol m^{-2} d^{-1}) are in accordance with global estimates of CO_2 emissions from desiccated sediments (mean (± SD) = 186 (± 326) mmol m^{-2} d^{-1}, median = 93 mmol m^{-2} d^{-1}) (Keller et al. 2020). The manually measured CO_2 fluxes are generally lower but comparable to CO_2 fluxes manually measured during the millennium drought in 2018 at the river Elbe (Mallast et al. 2020). The CO_2 fluxes from the automatic measurements show a greater variance and a higher mean, which is likely to derive from the higher temporal dynamics that were covered during automatic measurements.

4.1 The main source of CO_2 emissions

The sandy and therefore coarse texture of the unsaturated zone of the river sediments at the study site results in high water infiltration, evaporation and gas fluxes (Blume et al. 2016; Arce et al. 2019). Hence, it becomes likely that groundwater-borne CO_2 degasses where groundwater discharge hotpots are formed or where the groundwater level is close to the sediment surface (Macklin et al. 2014; Wood and Hyndman 2017; Mallast et al. 2020). Spatial dependence of high CO_2 fluxes close to the river was found by Mallast et al. (2020) during the millennium drought in 2018, suggesting degassing of groundwater-borne CO_2 close to the river, which attributes to the CO_2 emissions. This mechanism depends on the delayed response of the groundwater level to drought and the formation of a groundwater flow gradient towards the river (Peters et al. 2006; Tweed et al. 2009). Yet, a groundwater gradient was not observable at the study site, during periods of desiccation. Apart from this, increased fluxes with distance to the river were observed contrasting with the observations from Mallast et al. (2020) and the expectation that CO_2 derives from groundwater discharge hotspots close to the river. A spatial pattern of increased CO_2 emissions with distance to the river was also reported by Machado dos Santos Pinto et al. (2020) during periods of desiccation and is interpreted as differences in microbial activity and communities (Marxsen et al. 2010). Supporting this, results from the incubation experiments suggest that microbial respiration takes place at the study site. The production rates cover the magnitude of the fluxes measured in the field and are occasionally even higher. The bias is likely to be introduced by the sampling procedure of the incubations, causing changes in bulk density, aeration and “wall effects” which lead to altered gas fluxes during the laboratory experiment (Pell et al. 2005). In addition to that, the assumption that the production of CO_2 is uniform over the sediment column of the unsaturated zone might also lead

to an overestimation of the CO_2 fluxes. Higher production rates in September might be caused by the same effects, but might also derive from spatial and temporal heterogeneity of the sediment at the sampling site (Pell et al. 2005).

In soils, fluxes of heat, soil gas and water are interactive phenomena (Ouyang and Zheng 2000). Besides the observed gas fluxes, several observations e.g. diurnal pattern of soil moisture and a positive shift of water isotopes at the study site compared to the distant groundwater, suggest that evaporation takes place at the study site (Jackson 1973; Allison and Barnes 1983). Furthermore, shallow groundwater is likely to affect soil moisture and evaporation (Chen and Hu 2004). Based on this the amount of groundwater that would need to reach the sediment-atmosphere interphase and evaporate, to cover the measured CO_2 flux by degassing of groundwater-borne CO_2, was estimated. Modeled potential evaporation for Magdeburg show evaporation rates not significantly higher than 5 mm d^{-1} (LAU 2021), while estimates in this study suggest that 10 to 20 times higher evaporation rates would be needed if the CO_2 is entirely groundwater-born. Compared to the modeled potential evaporation these estimations provide maximum estimates of evaporation rates, due to simplification and assumptions. Nevertheless, the estimates are high for central Europe where evapotranspiration lies in a range of 250 to 500 mm yr^{-1} (Fohrer et al. 2016). Consequently, groundwater-born CO_2 might not be the main source of the CO_2 emissions, supporting previous results from incubation experiments.

Stable isotope composition and mixing models (Keeling plots) were applied to get further insights of sources and cycling of carbon at the study site (e.g. Keeling 1958; Cerling et al. 1991; Bowling et al. 2008) and yet show inconclusive results. Signatures of the CO_2 flux estimated with Keeling plots are the heaviest $\delta^{13}C$ signatures at the study site and differ significantly from the $\delta^{13}C$ signatures of the organic matter. However, the river and groundwater DIC signatures do not differ significantly from the CO_2 flux, which might indicate an influence of river and groundwater DIC on the CO_2 emissions. The DIC of open freshwater bodies is influenced by groundwater input, processes within rivers such as respiration and photosynthesis and equilibration with the atmosphere. Compared to the other endmember's the river $\delta^{13}DIC$ is enriched in ^{13}C, which can be caused by processes like photosynthesis and equilibration processes with the atmosphere, which are known to preferentially select lighter carbon, leading to enrichment of the remaining DIC (Yang et al. 1996; Doctor et al. 2008; Brunet et al. 2009). In contrast to that, groundwater $\delta^{13}DIC$ signature is depleted in ^{13}C. Compared to the river DIC, the groundwater DIC derives from microbial respiration in the sediment and dissolution of carbonate minerals (Schulte et al. 2011; Deirmendjian and Abril 2018). The comparable light groundwater $\delta^{13}DIC$ values might indicate that respired CO_2 from

the soil is the main source of the groundwater DIC (Schulte et al. 2011; Alemayehu et al. 2011). However, δ^{13}DIC in groundwater is likely to be influenced by diffusion and dissolution processes (Cerling et al. 1991; Alemayehu et al. 2011). The δ^{13}C sediment signatures are comparable to soil organic matter where the C3 photosynthetic pathway plays a major role (Cerling et al. 1991; O'Leary 1981). Respired soil CO_2 is likely to show similar δ^{13}C signatures as the soil organic matter (Peterson and Fry 1987; Cerling et al. 1991; Šantrůčková et al. 2000). The results of the Keeling plots however revealed CO_2 flux δ^{13}C signatures that are isotopic heavier than δ^{13}C signatures of the measured endmembers. Correcting for diffusive fractionation, based on Cerling et al. (1991), additionally increased the differences between flux and endmember δ^{13}C signatures. Therefore, the results of δ^{13}C signatures are not practicable to determine the CO_2 source at the study site. Supporting this, Nickerson and Risk (2009a, 2009b) showed that in diffusive environments assumptions of steady-state and linearity of Keeling plots are often violated. This leads to a misapplication of Keeling plots, which are based on linear regression, to non-linear mixing data. Consequently, this misapplication results in significant errors, more precisely a positive shift of the estimated CO_2 flux δ^{13}C signatures. The errors due to non-linearity depend on chamber height, soil characteristics and diffusive fractionation, and are likely to increase with increasing measurement time (Nickerson and Risk 2009a). Additionally, Risk and Kellman (2008) showed that diffusive fractionation during chamber measurements depends on concentration gradients and diffusivity and is therefore unlikely to be equivalent to the theoretical fractionation of – 4.4 ‰ as described in Cerling et al. (1991). Moreover, fractionation and mixing effects due to water sampling technique of river and groundwater based on headspace equilibration might also lead to biased δ^{13}DIC signatures of the endmembers. To achieve unbiased information about the δ^{13}C source signature corrections for non-linearity should be applied, diffusive fractionation needs to be analyzed in detail, unbiased river and groundwater δ^{13}DIC signatures need to be provided and a greater number of replicates should be taken in the field.

Since ^{222}Rn is not affected by biological processes but moves by the same mass flow and diffusion pathways that transport other soil gases, ^{222}Rn was used as a tracer for groundwater-borne CO_2 (Megonigal et al. 2020). The ^{222}Rn concentrations were significantly higher in groundwater and distant groundwater compared to the ^{222}Rn concentrations in the river, suggesting that the groundwater is likely to be a ^{222}Rn source (Genereux et al. 1993; Cook and Herczeg 2000). Additionally, soil emissions of ^{222}Rn were observed at the study site, suggesting diffusive or advective escape of ^{222}Rn from groundwater or soil gas into the atmosphere (Barbosa et al. 2010). Since ^{222}Rn moves by the same mass flow as CO_2 (Megonigal et al. 2020),

the expectation was that ^{222}Rn fluxes show the same spatial dependence as CO_2 fluxes if groundwater-borne CO_2 was the main source of the CO_2 emissions. Yet, in August sediment fluxes of ^{222}Rn are, in contrast to CO_2 fluxes, similar at each plot indicating uniform soil gas emissions over the whole study site, when CO_2 production by biological processes is disregarded. Observed ^{222}Rn fluxes in September however are higher where CO_2 fluxes are also high, suggesting that there is a temporal variability at the study site and that degassing groundwater is likely to increase the CO_2 emissions in September. To quantify if the groundwater degassing is significantly increasing the CO_2 flux is difficult since ^{222}Rn emissions from sandy substrate are low and the variability of the measured ^{222}Rn data high (Washington and Rose 1990). Additionally, the ^{222}Rn production of the unsaturated zone should be considered for quantification of the ^{222}Rn flux from the groundwater to estimate potential mixing effects (Schubert et al. 2020). Moreover, more replicates of ^{222}Rn flux measurements are recommended to get robust data, even though ^{222}Rn measurements were characterized by high variability.

While $\delta^{13}C$ results are biased and to be used with caution, ^{222}Rn flux measurements suggest that at least in September degassing CO_2 from the groundwater contributes to the CO_2 emissions. Yet, CO_2 fluxes in August are similar high. In combination with the missing groundwater gradient and high production rates from incubation experiments, these results suggest that microbial respiration is likely to be the main source of the CO_2 emissions and that degassing from the groundwater plays a minor role, regarding the CO2 emissions at the study site. A visual overview of these mechanisms is provided by Figure 15.

4.2 Influence of environmental variables on the CO_2 flux

Supporting hypothesis II) the organic matter content at the study site is generally low and does not seem to be a good predictor for the CO_2 fluxes. Microbial respiration is well-known to be controlled by organic matter availability (Marcé et al. 2019). Dry river sediments, however, contain generally lower, but therefore labile organic matter content, leading to high microbial activity even though organic matter quantity is low. Especially, in the first phase of drying autochthonous material from the previous flowing phase (e.g. biofilms and macrophytes) provides labile organic matter of high nutrient quality (Ylla et al. 2010; Gómez-Gener et al. 2016; Arce et al. 2019). Moreover, organic matter and nutrients are patchily distributed in dry river sediments as a result of downstream transport and deposition (Boix-Fayos et al. 2015; Stacy et al. 2015), which might lead to the measured spatial and temporal difference in organic matter content.

Mechanisms of sediment moisture controlling the CO_2 flux are complex. Increased sediment moisture can lead to increased solute transport and stimulation of microbial respiration on the one hand and limitation of gas diffusivity in the sediment on the other hand (Manzoni et al. 2012; Moyano et al. 2013; Gómez-Gener et al. 2016; Weise et al. 2016). The sediment moisture content at the study site is mainly controlled by sediment characteristics, evaporation, events of precipitation, rapid changes in water level and rise of groundwater (Chen and Hu 2004; Legates et al. 2011). A high correlation of decreasing soil moisture and increasing thickness of the unsaturated zone was observed, possibly indicating a causal relationship between soil moisture and thickness of the unsaturated zone (Chen and Hu 2004). Indeed, soil moisture and thickness of the unsaturated zone seem to be equally good predictors for CO_2 flux at the study site, indicating that an increased unsaturated zone and therefore dryer conditions lead to enhanced CO_2 emissions. Drying increases the air-filled pore space in the unsaturated zone which makes physical trapping of gases less likely and leads to enhanced aerobic respiration due to increased oxygen availability over the sediment column (Reverey et al. 2016; Machado dos Santos Pinto et al. 2020). The often-described effect of drought, reducing microbial activity due to substantial impacts on microbial physiology, was not observed at the study site. This implies that drying was not severe enough to affect the microbial activity, and suggests successive steps of drying with depth and time or rewetting by rise of groundwater, maintaining sufficient moisture content over the sediment column (Chen and Hu 2004; Marxsen et al. 2010; Manzoni et al. 2014; Weise et al. 2016). Altogether, the dependence of the CO_2 flux, increased unsaturated zone and drying, suggests that aerobic microbial respiration is likely to attribute to CO_2 emissions at the study site.

In general, the thickness of the unsaturated zone proofed to be a reasonably good predictor for CO_2 fluxes at the study site, suggesting that an increased unsaturated zone leads to increased microbial respiration and therefore higher CO_2 fluxes. As a first approach to quantify groundwater CO_2 emissions, the intercept of this linear model was used. The intercept provides the flux where the thickness of the unsaturated zone is zero and could therefore be interpreted as emissions from the groundwater. Based on this, a CO_2 flux from the groundwater of 7.5 mmol m^{-2} d^{-1} was estimated, which is comparatively low and cannot cover the observed CO_2 fluxes at the study site. Even though the model estimates are not significant and are just a snapshot from discrete measurements which might be influenced by many more factors, these results suggest that CO_2 fluxes from the groundwater have a considerable small impact on the CO_2 emissions at the study site.

Besides soil moisture and organic matter content, the temperature is known to control CO_2 production rates from dry sediment (Keller et al. 2020). Especially, soil respiration is highly influenced by soil temperature in absence of water stress (Kirschbaum 2000; Davidson et al. 2000). Indicators for temperature dependence are the well-known Q10 values, based on an exponential relationship of temperature and metabolic rates over a limited temperature range (Gillooly et al. 2001). However, activation energy can also be used to compare metabolic rates of biogeochemical processes (Gillooly et al. 2001; Dell et al. 2011). While changes in temperature during the manual measurements were not pronounced enough to show a temperature dependence of the CO_2 fluxes, the automatic measurements showed a stronger relation between CO_2 fluxes and temperature. The Q10 values and the activation energy from the incubation experiment and in the field were comparable to range and mean values from important metabolic reactions and soil respiration, proofing temperature dependence of CO_2 production and suggesting that microbial respiration takes place (Chen and Tian 2005; Dell et al. 2011). However, Q10 values slightly differed between the field measurements and the laboratory experiment. This might be the case since the estimation of Q10 of the field data is based on measured surface temperature while the measured surface flux is an integrated response to temperature across the soil profile, leading to inaccurate estimation of temperature sensitivity. Supporting this, a diurnal hysteresis relation was observed between soil temperature and CO_2. The hysteresis is likely to derive from a nonuniform soil temperature and production profile, caused by transport-related time lags of temperature and CO_2 through the profile, while measurements only take place at the sediment surface (Phillips et al. 2011). This is an often observed phenomenon (e.g. Riveros-Iregui et al. 2007; Bahn et al. 2008), explaining observed temporal time lags up to 4 hours between soil temperature and CO_2 flux, depending on physical soil characteristics (Phillips et al. 2011). Additionally, seasonal changes of soil moisture were found to influence time lags and hysteresis patterns due to opposing effects of soil moisture on heat and gas transport through a soil profile (Riveros-Iregui et al. 2007). This interaction of heat, water and gas flux makes it generally challenging to determine the influence of environmental variables (e.g. temperature) on the CO_2 flux by itself (Davidson et al. 2006; Phillips et al. 2011).

Altogether, the relationships between the environmental variables and the CO_2 flux support the earlier findings that microbial respiration is the main source of the CO_2 emissions at the study side and are therefore included in the visual overview provided by Figure 15.

Although dependences of drivers and fluxes could be identified, the variability of the data is still high and other factors are likely to additionally influence CO_2 emissions (Kim et al. 2012;

Rey 2015; Keller et al. 2020). For example, heavier events of precipitation (<1.5 mm) were observed to decrease CO_2 fluxes at the study site. Contrasting observations of a pulse of greenhouse gas emissions after precipitation events are found in arid regions. This is due to an increase of soil moisture and stimulation of microbial activity, also known as the "Birch-effect" (e.g. Huxman et al. 2004; Cable et al. 2008; Von Schiller et al. 2019). On the one hand, this suggests that drying at the study site is not severe enough to limit microbial respiration (Marxsen et al. 2010). On the other hand, the decreased CO_2 fluxes during and after precipitation suggest that infiltration and increased soil moisture content, lead to limitation of gas diffusivity (Moyano et al. 2013; Gómez-Gener et al. 2016). In addition to that, a decrease in soil temperature was observed after heavy rain events, indicating reduced microbial respiration due to the temperature response of the respiration processes (Ouyang and Zheng 2000). Apart from this, uptake of CO_2 from the sediment (negative fluxes) was observed close to the river, mainly during the day. At the same time, an undersaturation of dissolved CO_2 in the river was observed during the day, causing CO_2 uptake by the river, since emissions from streams mainly depend on the surface concentration and transfer coefficient (Halbedel and Koschorreck 2013). This observation leads to the assumption that close to the river CO_2 fluxes from the sediment might also be influenced by CO_2 emissions and uptake of the river water, for example, due to river water infiltration into the sediment. Admittedly, dissolved CO_2 was measured only over a few days simultaneously with the CO_2 fluxes from the sediment and more data would be needed to confirm this assumption.

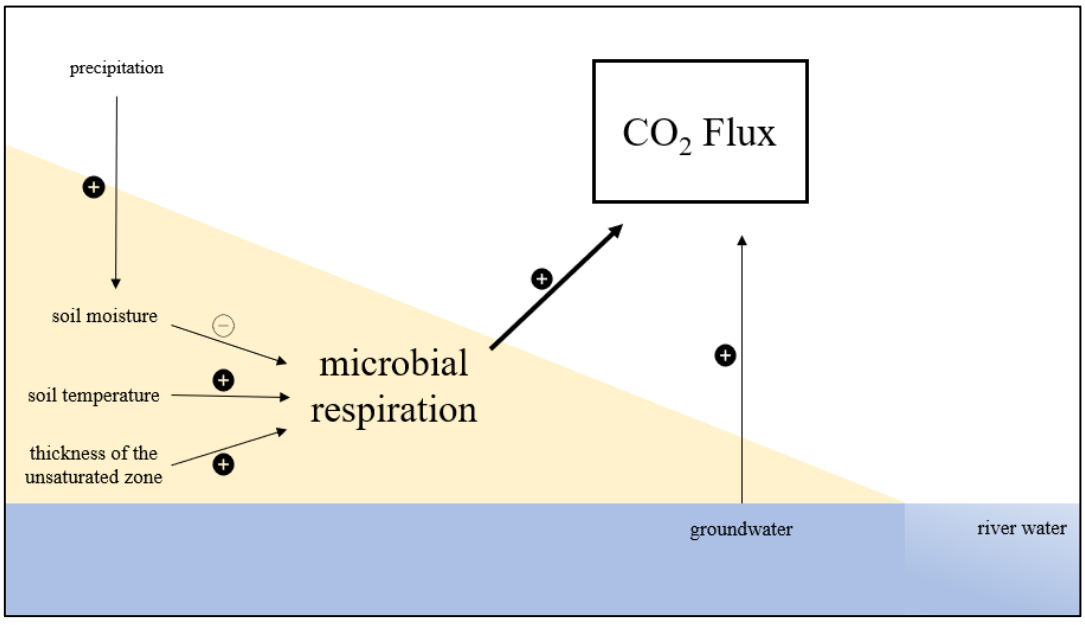

Figure 15: Schematic representation of the study site (cross section) with mechanisms that were found to influence the CO_2 fluxes. The font and arrow size indicate the importance of the mechanism. The (+) indicates an increase, while the (–) indicates a decrease.

5 Conclusion

The complementing set of methods that were applied provided no clear evidence that groundwater-borne CO_2 is the main source of CO_2 emissions. Contradicting to the hypothesis I), the results rather indicate that CO_2 from other sources, in particular microbial respiration, play a major role regarding the CO_2 emissions at the study site. This is supported by the observed spatial dependence, that CO_2 fluxes increase with distance to the river in combination with a missing hydrological gradient. Another, indication that microbial respiration contributes to CO_2 emissions at the study site, is provided by the results from the incubations, showing that production rates are high enough to cover measured fluxes and additionally revealing temperature dependence of the respiration process. Nevertheless, the measured data showed high temporal and spatial variability, reflecting the variability of environmental conditions, which might also lead to shifts and changes of sources and mechanisms of CO_2 emissions from the dry river sediments. For instance, a hydraulic gradient towards the river was observed, at the beginning of September during a period of rising water level. Additionally, ^{222}Rn emissions show temporal differences. The results from September indicate that groundwater-born CO_2 is likely to contribute to the CO_2 emissions, while results from August revealed rather low and uniform soil gas emissions over the study site if soil gas production by biological processes is disregarded.

The observed relations between environmental variables and CO_2 fluxes also indicate a high temporal and spatial variability and further suggest an influence of microbial respiration on CO_2 emissions from dry river sediments. Even though organic matter content was generally low, the organic matter in dry river sediments is commonly labile and of high nutrient quality and therefore fueling microbial respiration, especially in the first phase of drying (Ylla et al. 2010; Gómez-Gener et al. 2016; Arce et al. 2019). Moreover, the thickness of the unsaturated zone proofed to be a good predictor for CO_2 fluxes, which leads to the refutation of hypothesis II) that the unsaturated zone, more precisely the organic matter content and the thickness, does not influence the CO_2 flux.

First attempts to quantify CO_2 emissions from different sources, revealed high production rates of CO_2 from microbial respiration and comparable low CO_2 emissions from groundwater, indicating that groundwater-borne CO_2 is not likely to affect CO_2 emissions at the study site.

Based on the gained evidence, we assume that the CO_2 emissions from dry sediments at the river Elbe, mainly derive from microbial respiration. However, the results also showed that mechanisms and relations are complex and that further investigation is needed. Especially with the focus on quantifying emissions from different sources, analysis of stable water and carbon

isotopes and ^{222}Rn, could be used for detailed mixing models. Therefore, information of additional endmembers, diffusion coefficients and corrections for diffusive environments would be needed (Nickerson and Risk 2009a; Schubert 2015; Megonigal et al. 2020). Additionally, higher temporal and spatial resolution data and more importantly repetition in following years, with severe droughts over summer, might help to find out if mechanisms are consistent and deepen the understanding of mechanisms behind CO_2 emissions from dry sediments of high-order rivers.

Acknowledgment

First of all, I would like to thank Prof. Dr. Klaus-Holger Knorr for the support and advice throughout the duration of the thesis.

I would also like to thank Dr. Matthias Koschorreck for the opportunity to write my master thesis in cooperation with the Helmholtz Centre of Environmental Research and for the constant guidance and support especially in the early stage of preparation, during the field work and data analysis.

Moreover, I would like to thank the technical personnel of the Helmholtz Centre of Environmental Research and the Westfälische Wilhelms-University for their help during the work in the field and in the laboratory. I am especially grateful to Martin Wieprecht for his help and support during the field work and to Corinna Völkner for her help and instructions in the laboratory. Additionally, I would like to thank Ulrike Berning-Mader, Ines Locker and Andrea Hoff for their support in the laboratory.

Many thanks go to the whole working group Lake Microbiology of the Helmholtz Centre of Environmental Research who welcomed and supported me in Magdeburg on both a professional and a personal level. I would also like to thank the working group ecohydrology and biogeochemistry of the Westfälische Wilhelms-University for helping me with the organization and data analysis.

Finally, I thank my friends and family, especially Maiken Baumberger, Lukáš Vrba, Lukas Fuhse and Sage Claughton for their encouragement and help during writing the thesis.

References

Alemayehu, T.; Leis, A.; Eisenhauer, A.; Dietzel, M. (2011): Multi-proxy approach ($^{2}H/H$, $^{18}O/^{16}O$, $^{13}C/^{12}C$ and $^{87}Sr/^{86}Sr$) for the evolution of carbonate-rich groundwater in basalt dominated aquifer of Axum area, northern Ethiopia. In *Geochemistry* 71 (2), pp. 177–187. DOI: 10.1016/j.chemer.2011.02.007.

Allison, G. B.; Barnes, C. J. (1983): Estimation of evaporation from non-vegetated surfaces using natural deuterium. In *Nature* 301 (5896), pp. 143–145. DOI: 10.1038/301143a0.

Arce, M. I.; Mendoza-Lera, C.; Almagro, M.; Catalán, N.; Romaní, A. M.; Martí, Eugènia et al. (2019): A conceptual framework for understanding the biogeochemistry of dry riverbeds through the lens of soil science. In *Earth-Science Reviews* 188, pp. 441–453. DOI: 10.1016/j.earscirev.2018.12.001.

Bahn, M.; Rodeghiero, M.; Anderson-Dunn, M.; Dore, S.; Gimeno, C.; Drösler, M. et al. (2008): Soil Respiration in European Grasslands in Relation to Climate and Assimilate Supply. In *Ecosystems* 11 (8), pp. 1352–1367. DOI: 10.1007/s10021-008-9198-0.

Barbosa, S. M.; Zafrir, H.; Malik, U.; Piatibratova, O. (2010): Multiyear to daily radon variability from continuous monitoring at the Amram tunnel, southern Israel. In *Geophysical Journal International* 182 (2), pp. 829–842. DOI: 10.1111/j.1365-246X.2010.04660.x.

Battin, T. J.; Kaplan, L. A.; Findlay, S.; Hopkinson, C. S.; Marti, E.; Packman, A. I. et al. (2008): Biophysical controls on organic carbon fluxes in fluvial networks. In *Nature Geoscience* 1 (2), pp. 95–100. DOI: 10.1038/ngeo101.

Blume, H.-P.; Brümmer, G. W.; Fleige, H.; Horn, R.; Kandeler, E.; Kögel-Knabner, I. et al. (2016): Scheffer/Schachtschabel Soil Science. Berlin, Heidelberg: Springer. DOI: 10.1007/978-3-642-30942-7.

Boessenkool, Berry (2020): rdwd: Select and Download Climate Data from 'DWD' (German Weather Service). Version R package version 1.3.1. Available online at https://CRAN.R-project.org/package=rdwd, checked on 11/8/2020.

Boix-Fayos, C.; Nadeu, E.; Quiñonero, J. M.; Martínez-Mena, M.; Almagro, M.; Vente, J. de (2015): Sediment flow paths and associated organic carbon dynamics across a Mediterranean catchment. In *Hydrology and Earth System Sciences* 19 (3), pp. 1209–1223. DOI: 10.5194/hess-19-1209-2015.

Bolpagni, R.; Laini, A.; Mutti, T.; Viaroli, P.; Bartoli, M. (2019): Connectivity and habitat typology drive CO_2 and CH_4 fluxes across land-water interfaces in lowland rivers. In *Ecohydrology* 12 (1), e2036. DOI: 10.1002/eco.2036.

Bowling, D. R.; Pataki, D. E.; Randerson, J. T. (2008): Carbon isotopes in terrestrial ecosystem pools and CO_2 fluxes. In *The New phytologist* 178 (1), pp. 24–40. DOI: 10.1111/j.1469-8137.2007.02342.x.

Brunet, F.; Dubois, K.; Veizer, J.; Nkoue Ndondo, G. R.; Ndam Ngoupayou, J. R.; Boeglin, J. L.; Probst, J. L. (2009): Terrestrial and fluvial carbon fluxes in a tropical watershed: Nyong basin, Cameroon. In *Chemical Geology* 265 (3-4), pp. 563–572. DOI: 10.1016/j.chemgeo.2009.05.020.

Cable, J. M.; Ogle, K.; Williams, D. G.; Weltzin, J. F.; Huxman, T. E. (2008): Soil Texture Drives Responses of Soil Respiration to Precipitation Pulses in the Sonoran Desert: Implications for Climate Change. In *Ecosystems* 11 (6), pp. 961–979. DOI: 10.1007/s10021-008-9172-x.

Cerling, T. E.; Solomon, D. K.; Quade, J.; Bowman, J. R. (1991): On the isotopic composition of carbon in soil carbon dioxide. In *Geochimica et Cosmochimica Acta* 55 (11), pp. 3403–3405. DOI: 10.1016/0016-7037(91)90498-T.

Chen, H.; Tian, H.-Q. (2005): Does a General Temperature-Dependent Q10 Model of Soil Respiration Exist at Biome and Global Scale? In *Journal of Integrative Plant Biology* 47 (11), pp. 1288–1302. DOI: 10.1111/j.1744-7909.2005.00211.x.

Chen, X.; Hu, Q. (2004): Groundwater influences on soil moisture and surface evaporation. In *Journal of Hydrology* 297 (1), pp. 285–300. DOI: 10.1016/j.jhydrol.2004.04.019.

Cook, P. G.; Herczeg, A. L. (2000): Environmental Tracers in Subsurface Hydrology. Boston, MA: Springer US. DOI: 10.1007/978-1-4615-4557-6.

Cook, P. G.; Wood, C.; White, T.; Simmons, C. T.; Fass, T.; Brunner, P. (2008): Groundwater inflow to a shallow, poorly-mixed wetland estimated from a mass balance of radon. In *Journal of Hydrology* 354 (1-4), pp. 213–226. DOI: 10.1016/j.jhydrol.2008.03.016.

Coppola, E.; Verdecchia, M.; Giorgi, F.; Colaiuda, V.; Tomassetti, B.; Lombardi, A. (2014): Changing hydrological conditions in the Po basin under global warming. In *Science of The Total Environment* 493, pp. 1183–1196. DOI: 10.1016/j.scitotenv.2014.03.003.

Davidson, E. A.; Trumbore, S. E.; Amundson, R. (2000): Soil warming and organic carbon content. In *Nature* 408 (6814), pp. 789–790. DOI: 10.1038/35048672.

Davidson, E. A.; Janssens, I. A.; Luo, Y. (2006): On the variability of respiration in terrestrial ecosystems. Moving beyond Q10. In *Global Change Biology* 12 (2), pp. 154–164. DOI: 10.1111/j.1365-2486.2005.01065.x.

Deirmendjian, L.; Abril, G. (2018): Carbon dioxide degassing at the groundwater-stream-atmosphere interface: isotopic equilibration and hydrological mass balance in a sandy watershed. In *Journal of Hydrology* 558, pp. 129–143. DOI: 10.1016/j.jhydrol.2018.01.003.

Del Giorgio, P. A.; Pace, M. L. (2008): Relative independence of organic carbon transport and processing in a large temperate river. The Hudson River as both pipe and reactor. In *Limnology and Oceanography* 53 (1), pp. 185–197. DOI: 10.4319/lo.2008.53.1.0185.

Dell, Anthony I.; Pawar, Samraat; van Savage, M. (2011): Systematic variation in the temperature dependence of physiological and ecological traits. In *Proceedings of the National Academy of Sciences of the United States of America* 108 (26), pp. 10591–10596. DOI: 10.1073/pnas.1015178108.

Deutscher Wetterdienst (2020): Datenbasis. Einzelwerte gemittelt. Available online at ftp://opendata.dwd.de/climate_environment/CDC/observations_germany/climate/hourly/, checked on 3/3/2020.

Doctor, D. H.; Kendall, C.; Sebestyen, S. D.; Shanley, J. B.; Ohte, N.; Boyer, E. W. (2008): Carbon isotope fractionation of dissolved inorganic carbon (DIC) due to outgassing of carbon dioxide from a headwater stream. In *Hydrological Processes* 22 (14), pp. 2410–2423. DOI: 10.1002/hyp.6833.

DURRIDGE (2021): RAD7 Radon Detector. User Manual. USA. Available online at https://durridge.com/documentation/RAD7%20Manual.pdf, checked on 3/3/2020.

Fohrer, N.; Bormann, H.; Miegel, K.; Casper, M. (2016): Hydrologie. Stuttgart: UTB.

Gasmet Technologies GmbH (2018): FTIR-Gasanalysator DX4000. Finland. Available online at https://www.gasmet.com/de/wp-content/uploads/sites/6/2018/01/Gasmet-DX4000-Technical-Data-v1.10.pdf, checked on 3/3/2020.

Genereux, D. P.; Hemond, H. F.; Mulholland, P. J. (1993): Use of radon-222 and calcium as tracers in a three-end-member mixing model for streamflow generation on the West Fork

of Walker Branch Watershed. In *Journal of Hydrology* 142 (1-4), pp. 167–211. DOI: 10.1016/0022-1694(93)90010-7.

Gillooly, J. F.; Brown, J. H.; West, G. B.; Savage, V. M.; Charnov, E. L. (2001): Effects of size and temperature on metabolic rate. In *Science* 293 (5538), pp. 2248–2251. DOI: 10.1126/science.1061967.

Gómez-Gener, L.; Obrador, B.; Marcé, R.; Acuña, V.; Catalán, N.; Casas-Ruiz, J. P. et al. (2016): When Water Vanishes: Magnitude and Regulation of Carbon Dioxide Emissions from Dry Temporary Streams. In *Ecosystems* 19 (4), pp. 710–723. DOI: 10.1007/s10021-016-9963-4.

Gómez-Gener, L.; Obrador, B.; Von Schiller, D.; Marcé, R.; Casas-Ruiz, J. P.; Proia, L. et al. (2015): Hot spots for carbon emissions from Mediterranean fluvial networks during summer drought. In *Biogeochemistry* 125 (3), pp. 409–426. DOI: 10.1007/s10533-015-0139-7.

Gustafsson, J. P. (2020): Visual MINTEQ. Version 3.1. Sweden. Available online at https://vminteq.lwr.kth.se/, checked on 3/3/2020.

Halbedel, S.; Koschorreck, M. (2013): Regulation of CO_2 emissions from temperate streams and reservoirs. In *Biogeosciences* 10 (11), pp. 7539–7551. DOI: 10.5194/bg-10-7539-2013.

Huxman, T. E.; Snyder, K. A.; Tissue, D.; Leffler, A. J.; Ogle, K.; Pockman, W. T. et al. (2004): Precipitation pulses and carbon fluxes in semiarid and arid ecosystems. In *Oecologia* 141 (2), pp. 254–268. DOI: 10.1007/s00442-004-1682-4.

Hvorslev, M. J. (1951): Time lag and soil permeability in ground-water observations. Waterways Experiment Station, Corps of Engineers, US Army (36).

Jackson, R. D. (1973): Diurnal changes in soil water content during drying. In *Field soil water regime* 5, pp. 37–55. DOI: 10.2136/sssaspecpub5.c3

Keeling, C. D. (1958): The concentration and isotopic abundances of atmospheric carbon dioxide in rural areas. In *Geochimica et Cosmochimica Acta* 13 (4), pp. 322–334. DOI: 10.1016/0016-7037(58)90033-4.

Keller, P. S. (2020): glimmr: Compute gasfluxes with R. Gas Fluxes and Dynamic Chamber Measurements. Version 0.1.0.9000 (unreleased). Available online at https://github.com/tekknosol/glimmr, checked on 3/4/2020.

Keller, P. S.; Catalán, N.; Von Schiller, D.; Grossart, H.-P.; Koschorreck, M.; Obrador, B. et al. (2020): Global CO_2 emissions from dry inland waters share common drivers across ecosystems. In *Nature Communications* 11 (1), pp. 1–8. DOI: 10.1038/s41467-020-15929 - y.

Kim, D.-G.; Vargas, R.; Bond-Lamberty, B.; Turetsky, M. R. (2012): Effects of soil rewetting and thawing on soil gas fluxes: a review of current literature and suggestions for future research. In *Biogeosciences* 9 (7), pp. 2459–2483. DOI: 10.5194/bg-9-2459-2012.

Kim, J.; Lee, S.-S.; Ha, S.-W.; Joun, W.-T.; Ju, Y.; Lee, K.-K. (2020): Natural ^{222}Rn as a tracer of mixing and volatilization in a shallow aquifer during a CO_2 injection experiment. In *Hydrological Processes* 34 (26), pp. 5417–5428. DOI: 10.1002/hyp.13953.

Kirschbaum, M. U. F. (2000): Will changes in soil organic carbon act as a positive or negative feedback on global warming? In *Biogeochemistry* 48 (1), pp. 21–51. DOI: 10.1023/A:1006238902976.

Koschorreck, M.; Prairie, Y. T.; Kim, J.; Marcé, R. (2020): Technical note. CO_2 is not like CH_4 – limits of and corrections to the headspace method to analyse pCO_2 in water. In Biogeosciences 18 (5), pp. 1619–1627. DOI: 10.5194/bg-18-1619-2021.

LAU (2021): ReKIS. Regionales Klimainformationssystem für Sachsen, Sachsen-Anhalt und Thüringen. Edited by Landesamt für Umweltschutz Sachsen-Anhalt. Available online at https://rekisviewer.hydro.tu-dresden.de/fdm/ReKISExpert.jsp#menu-2, checked on 3/29/2020.

Legates, D. R.; Mahmood, R.; Levia, D. F.; DeLiberty, T. L.; Quiring, S. M.; Houser, C.; Nelson, F. E. (2011): Soil moisture: A central and unifying theme in physical geography. In *Progress in Physical Geography: Earth and Environment* 35 (1), pp. 65–86. DOI: 10.1177/0309133310386514.

Leyer, I.; Wesche, K. (2007): Multivariate Statistik in der Ökologie. Eine Einführung. Berlin: Springer. DOI: 10.1007/978-3-540-37706-1

LHW (2020): Flood warning system of the State of Saxony-Anhalt. Available online at https://hochwasservorhersage.sachsen-anhalt.de/messwerte/wasserstand/?no_cache=1, checked on 3/3/2020.

Looman, A.; Maher, D. T.; Pendall, E.; Bass, A.; Santos, I. R. (2017): The carbon dioxide evasion cycle of an intermittent first-order stream. Contrasting water–air and soil–air exchange. In *Biogeochemistry* 132 (1-2), pp. 87–102. DOI: 10.1007/s10533-016-0289-2.

Machado dos Santos Pinto, R.; Weigelhofer, G.; Diaz-Pines, E.; Guerreiro Brito, A.; Zechmeister-Boltenstern, S.; Hein, T. (2020): River-floodplain restoration and hydrological effects on GHG emissions. Biogeochemical dynamics in the parafluvial zone. In *Science of The Total Environment* 715, p. 136980. DOI: 10.1016/j.scitotenv.2020.136980.

Macklin, P. A.; Maher, D. T.; Santos, I. R. (2014): Estuarine canal estate waters. Hotspots of CO_2 outgassing driven by enhanced groundwater discharge? In *Marine Chemistry* 167, pp. 82–92. DOI: 10.1016/j.marchem.2014.08.002.

Macpherson, G. L. (2009): CO_2 distribution in groundwater and the impact of groundwater extraction on the global C cycle. In *Chemical Geology* 264 (1-4), pp. 328–336. DOI: 10.1016/j.chemgeo.2009.03.018.

Mallast, U.; Staniek, M.; Koschorreck, M. (2020): Spatial upscaling of CO_2 emissions from exposed river sediments of the Elbe River during an extreme drought. In *Ecohydrology 13 (6)*, e2216. *DOI:* 10.1002/eco.2216.

Manzoni, S.; Schimel, J. P.; Porporato, A. (2012): Responses of soil microbial communities to water stress. Results from a meta-analysis. In *Ecology* 93 (4), pp. 930–938. DOI: 10.1890/11-0026.1.

Manzoni, S.; Schaeffer, S. M.; Katul, G.; Porporato, A.; Schimel, J. P. (2014): A theoretical analysis of microbial eco-physiological and diffusion limitations to carbon cycling in drying soils. In *Soil biology & biochemistry* 73, pp. 69–83. DOI: 10.1016/j.soilbio.2014.02.008.

Marcé, R.; Obrador, B.; Gómez-Gener, L.; Catalán, N.; Koschorreck, M.; Arce, M. I. et al. (2019): Emissions from dry inland waters are a blind spot in the global carbon cycle. In *Earth-Science Reviews* 188, pp. 240–248. DOI: 10.1016/j.earscirev.2018.11.012.

Marxsen, J.; Zoppini, A.; Wilczek, S. (2010): Microbial communities in streambed sediments recovering from desiccation. In *FEMS microbiology ecology* 71 (3), pp. 374–386. DOI: 10.1111/j.1574-6941.2009.00819.x.

Megonigal, J. P.; Brewer, P. E.; Knee, K. L. (2020): Radon as a natural tracer of gas transport through trees. In *The New phytologist* 225 (4), pp. 1470–1475. DOI: 10.1111/nph.16292.

Moyano, F. E.; Manzoni, S.; Chenu, C. (2013): Responses of soil heterotrophic respiration to moisture availability: An exploration of processes and models. In *Soil biology & biochemistry* 59, pp. 72–85. DOI: 10.1016/j.soilbio.2013.01.002.

Nickerson, N.; Risk, D. (2009a): Keeling plots are non-linear in non-steady state diffusive environments. In *Geophysical Research Letters* 36 (8), p. 83. DOI: 10.1029/2008GL036945.

Nickerson, N.; Risk, D. (2009b): Physical controls on the isotopic composition of soil-respired CO_2. In *JGR Biogeosciences.* 114 (G1), p. 83. DOI: 10.1029/2008JG000766.

O'Leary, M. H. (1981): Carbon isotope fractionation in plants. In *Phytochemistry* 20 (4), pp. 553–567. DOI: 10.1016/0031-9422(81)85134-5.

Ouyang, Y.; Zheng, C. (2000): Surficial processes and CO_2 flux in soil ecosystem. In *Journal of Hydrology* 234 (1-2), pp. 54–70. DOI: 10.1016/S0022-1694(00)00240-7.

Pell, M.; Stenström, J.; Granhall, U. (2005): Soil Respiration. In *Microbiological Methods for Assessing Soil Quality*, Bloem, J.; D.W. Hopkins & A. Benedetti, pp. 117–126. Boston, MA, USA: CAB International.

Peters, E.; Bier, G.; van Lanen, H.A.J.; Torfs, P.J.J.F. (2006): Propagation and spatial distribution of drought in a groundwater catchment. In *Journal of Hydrology* 321 (1-4), pp. 257–275. DOI: 10.1016/j.jhydrol.2005.08.004.

Peterson, B. J.; Fry, B. (1987): Stable isotopes in ecosystem studies. In *Annual review of ecology and systematics* 18 (1), pp. 293–320.

Phillips, C. L.; Nickerson, N.; Risk, D.; Bond, B. J (2011): Interpreting diel hysteresis between soil respiration and temperature. In *Global Change Biology* 17 (1), pp. 515–527. DOI: 10.1111/j.1365-2486.2010.02250.x.

PP Systems (2018): CFLUX-1 Automated Soil CO2 Flux System. USA. Available online at https://ppsystems.com/wp-content/uploads/EDSCFLUX1.pdf, checked on 3/3/2020.

PP Systems (2020): EGM-5 Portable CO2 Gas Analyzer. USA. Available online at https://ppsystems.com/wp-content/uploads/EDSEGM5_1120.pdf, checked on 3/3/2020.

Reverey, F.; Grossart, H.-P.; Premke, K.; Lischeid, G. (2016): Carbon and nutrient cycling in kettle hole sediments depending on hydrological dynamics: a review. In *Hydrobiologia* 775 (1), pp. 1–20. DOI: 10.1007/s10750-016-2715-9.

Rey, A. (2015): Mind the gap. Non-biological processes contributing to soil CO_2 efflux. In *Global change biology* 21 (5), pp. 1752–1761. DOI: 10.1111/gcb.12821.

Risk, D.; Kellman, L. (2008): Isotopic fractionation in non-equilibrium diffusive environments. In *Geophysical Research Letters* 35 (2), p. 57. DOI: 10.1029/2007GL032374.

Riveros-Iregui, D. A.; Emanuel, R. E.; Muth, D. J.; McGlynn, B. L.; Epstein, H. E.; Welsch, D. L. et al. (2007): Diurnal hysteresis between soil CO_2 and soil temperature is controlled by soil water content. In *Geophys. Res. Lett.* 34 (17). DOI: 10.1029/2007GL030938.

Samaniego, L.; Thober, S.; Kumar, R.; Wanders, N.; Rakovec, O.; Pan, M. et al. (2018): Anthropogenic warming exacerbates European soil moisture droughts. In *Nature Climate Change* 8 (5), pp. 421–426. DOI: 10.1038/s41558-018-0138-5.

Sander, R. (2015): Compilation of Henry's law constants (version 4.0) for water as solvent. In *Atmos. Chem. Phys.* 15 (8), pp. 4399–4981. DOI: 10.5194/acp-15-4399-2015.

Šantrůčková, H.; Bird, M. I.; Lloyd, J. (2000): Microbial processes and carbon-isotope fractionation in tropical and temperate grassland soils. In *Functional Ecology* 14 (1), pp. 108–114. DOI: 10.1046/j.1365-2435.2000.00402.x.

Von Schiller, D.; Datry, T.; Corti, R.; Foulquier, A.; Tockner, K.; Marcé, R. et al. (2019): Sediment Respiration Pulses in Intermittent Rivers and Ephemeral Streams. In *Global Biogeochemical Cycles* 33 (10), pp. 1251–1263. DOI: 10.1029/2019GB006276.

Von Schiller, D.; Marcé, R.; Obrador, B.; Gómez-Gener, L.; Casas-Ruiz, J. P.; Acuña, V.; Koschorreck, M. (2014): Carbon dioxide emissions from dry watercourses. In *Inland Waters* 4 (4), pp. 377–382. DOI: 10.5268/IW-4.4.746.

Schlesinger, W. H.; Melack, J. M. (1981): Transport of organic carbon in the world's rivers. In *Tellus* 33 (2), pp. 172–187. DOI: 10.3402/tellusa.v33i2.10706.

Scholten, M.; Anlauf, A.; Büchele, B.; Faulhaber, P.; Henle, K.; Kofalk, S. et al. (2003): The River Elbe in Germany - present state, conflicting goals, and perspectives of rehabilitation. In *Large Rivers* 15 (1-4), pp. 579–602. DOI: 10.1127/lr/15/2003/579.

Scholz, M.; Schwartz, R.; Weber, M. (2005): Flusslandschaft Elbe – Entwicklung und heutiger Zustand In *Lebensräume der Elbe und ihrer Auen*, Scholz, M.; Stab, S.; Dziock, F.& K. Henle, pp. 5–48. Berlin: Weißensee Verlag.

Schubert, M. (2015): Using radon as environmental tracer for the assessment of subsurface Non-Aqueous Phase Liquid (NAPL) contamination – A review. In *European Physical Journal Special Topics* 224 (4), pp. 717–730. DOI: 10.1140/epjst/e2015-02402-3.

Schubert, M.; Knoeller, K.; Mueller, C.; Gilfedder, B. (2020): Investigating River Water/Groundwater Interaction along a Rivulet Section by ^{222}Rn Mass Balancing. In *Water* 12 (11), p. 3027. DOI: 10.3390/w12113027.

Schulte, P.; Van Geldern, R.; Freitag, H.; Karim, A.; Négrel, P.; Petelet-Giraud, E. et al. (2011): Applications of stable water and carbon isotopes in watershed research. Weathering, carbon cycling, and water balances. In *Earth-Science Reviews* 109 (1-2), pp. 20–31. DOI: 10.1016/j.earscirev.2011.07.003.

Sigg, L.; Stumm, W. (2016): Aquatische Chemie. Einführung in die Chemie natürlicher Gewässer. Zürich: vdf Hochschulverlag AG an der ETH Zürich.

Spinoni, J.; Vogt, J. V.; Naumann, G.; Barbosa, P.; Dosio, A. (2018): Will drought events become more frequent and severe in Europe? In *International Journal of Climatology* 38 (4), pp. 1718–1736. DOI: 10.1002/joc.5291.

Stacy, E. M.; Hart, S. C.; Hunsaker, C. T.; Johnson, D. W.; Berhe, A. A. (2015): Soil carbon and nitrogen erosion in forested catchments: implications for erosion-induced terrestrial carbon sequestration. In *Biogeosciences* 12 (16), pp. 4861–4874. DOI: 10.5194/bg-12-4861-2015.

Steward, A. L.; Von Schiller, D.; Tockner, K.; Marshall, J. C.; Bunn, S. E. (2012): When the river runs dry. Human and ecological values of dry riverbeds. In *Frontiers in Ecology and the Environment* 10 (4), pp. 202–209. DOI: 10.1890/110136.

Tweed, S.; Leblanc, M.; Cartwright, I. (2009): Groundwater–surface water interaction and the impact of a multi-year drought on lakes conditions in South-East Australia. In *Journal of Hydrology* 379 (1-2), pp. 41–53. DOI: 10.1016/j.jhydrol.2009.09.043.

UNESCO/IHA (2010): GHG Measurement Guidelines for Freshwater Reservoirs. London: The International Hydropower Association (IHA).

Washington, J. W.; Rose, A. W. (1990): Regional and temporal relations of radon in soil gas to soil temperature and moisture. In *Geophysical Research Letters* 17 (6), pp. 829–832. DOI: 10.1029/GL017i006p00829.

Weigold, F.; Baborowski, M. (2009): Consequences of delayed mixing for quality assessment of river water. Example Mulde–Saale–Elbe. In *Journal of Hydrology* 369 (3), pp. 296–304. DOI: 10.1016/j.jhydrol.2009.02.039.

Weise, L.; Ulrich, A.; Moreano, M.; Gessler, A.; Kayler, Z. E.; Steger, K. et al. (2016): Water level changes affect carbon turnover and microbial community composition in lake sediments. In *FEMS microbiology ecology* 92 (5), fiw035. DOI: 10.1093/femsec/fiw035.

Wood, W. W.; Hyndman, D. W. (2017): Groundwater Depletion: A Significant Unreported Source of Atmospheric Carbon Dioxide. In *Earth's Future* 5 (11), pp. 1133–1135. DOI: 10.1002/2017EF000586.

WSV (2020): ELWIS. Wasserstände & Vorhersagen an schifffahrtsrelevanten Pegeln. Pegel Magdeburg-Strombrücke. Wasserstraßen- und Schifffahrtsverwaltung des Bundes (WSV) im Geschäftsbereich des Bundesministeriums für Verkehr und digitale Infrastruktur (BMVI). Available online at https://www.elwis.de/DE/dynamisch/gewaesserkunde/wasserstaende/index.php?target=1&pegelId=ccccb57f-a2f9-4183-ae88-5710d3afaefd, checked on 11/8/2020.

Yang, C.; Telmer, K.; Veizer, J. (1996): Chemical dynamics of the "St. Lawrence" riverine system: δD_{H2O}, $\delta^{18}O_{H2O}$, $\delta^{13}C_{DIC}$, $\delta^{34}S_{sulfate}$, and dissolved $^{87}Sr/^{86}Sr$. In *Geochimica et Cosmochimica Acta* 60 (5), pp. 851–866. DOI: 10.1016/0016-7037(95)00445-9.

Ylla, I.; Sanpera-Calbet, I.; Vázquez, E.; Romaní, A. M.; Muñoz, I.; Butturini, A.; Sabater, S. (2010): Organic matter availability during pre- and post-drought periods in a Mediterranean stream. In *Hydrobiologia* 657 (1), pp. 217–232. DOI: 10.1007/s10750-010-0193-z.

Appendix

Table A1: The measured $\delta^{18}O$ and $\delta^{2}H$ signatures of the groundwater (GW), river water (EW) and distant groundwater (dGW).

Date	Sample	Distance [m]	$\delta^{2}H$ (±SD) [‰]	$\delta^{18}O$ (±SD) [‰]
2020-08-04	GW	1	-58.7 (2.0)	-7.9 (0.3)
2020-08-04	GW	3	-56.0 (2.4)	-7.6 (0.2)
2020-08-04	GW	5	-57.8 (0.6)	-7.9 (0.1)
2020-08-04	GW	6	-56.6 (2.5)	-7.8 (0.2)
2020-08-04	EW	0	-59.1 (1.3)	-8.0 (0.2)
2020-09-23	GW	1	-56.9 (1.2)	-7.7 (0.2)
2020-09-23	GW	2	-57.0 (2.1)	-7.7 (0.3)
2020-09-23	GW	3	-57.6 (0.9)	-7.8 (0.1)
2020-09-23	GW	4	-56.8 (3.1)	-7.8 (0.4)
2020-09-23	EW	0	-58.6 (0.5)	-8.0 (0.001)
2020-09-07	dGW	500	-63.5 (2.6)	-9.0 (0.2)
2020-09-07	dGW	2000	-59.9 (2.7)	-8.4 (0.3)

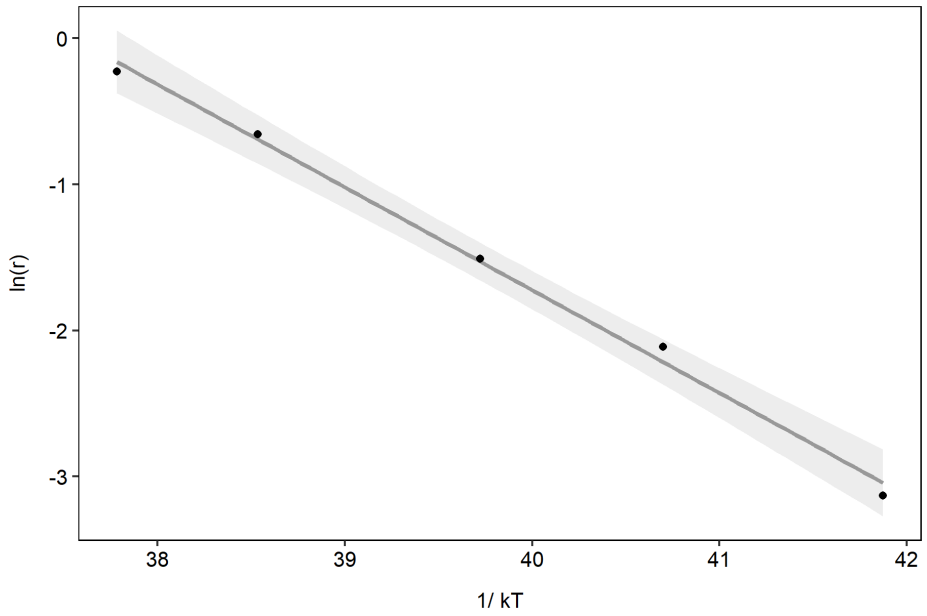

Figure A1: Arrhenius plot based on the data from the incubation experiment in laboratory. The natural logarithm of the production rate (ln(r)) plotted against the reciprocal of the Boltzmann constant (k) × Temperature (T).

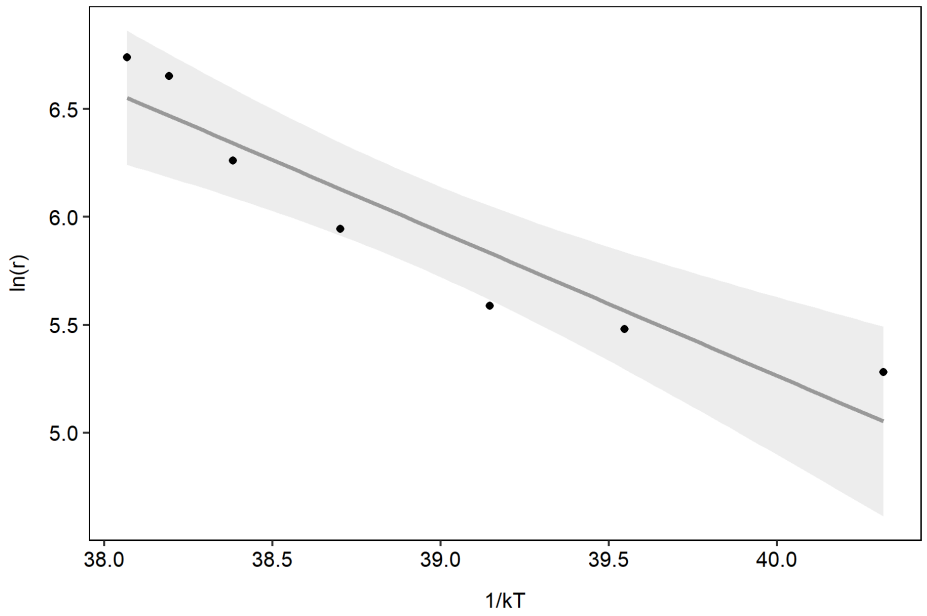

Figure A2: Arrhenius plot based on the data from the automatic measurements in the field. The natural logarithm of the production rate (ln(r)) plotted against the reciprocal of the Boltzmann constant (k) × Temperature (T).

Table A2: Additional chemical and physical parameters of the groundwater (GW), the river water (EW), and the distant groundwater (dGW).

Date	Sample	Distance [m]	Temperature [°C]	Conductivity [µS cm^{-1}]	pH	O_2 [%]	O_2 [mg L^{-1}]
2020-08-04	GW	1	19.4	610	7.2	9.2	0.82
2020-08-04	GW	3	19.9	658	6.8	12.1	1.07
2020-08-04	GW	5	19.0	640	6.6	21.5	1.92
2020-08-04	GW	6	20.3	1563	6.6	23	2
2020-08-04	EW	0	21.1	640	8.3	102.4	9.1
2020-08-04	EW	0	22.0	635	8.3	111.5	9.58
2020-08-04	EW	0	22.7	645	8.6	128.4	11.06
2020-09-02	GW	2	19.0	758	-	-	0.5
2020-09-02	GW	3	19.1	815	-	-	1.25
2020-09-02	EW	0	19.0	703	-	-	9.5
2020-09-07	dGW	2000	16.0	1043	7.1	57.2	5.37
2020-09-07	dGW	500	19.5	760	6.9	42.4	3.9
2020-09-23	GW	1	16.5	696	7.2	35.5	3.4
2020-09-23	GW	2	16.1	655	7.3	25.6	2.47
2020-09-23	GW	3	16.8	647	7.2	41	3.98
2020-09-23	GW	4	17.3	640	7.0	41.3	3.95
2020-09-23	EW	0	18.2	601	8.0	99.3	9.27
2020-09-23	EW	0	18.3	601	8.1	101	9.42
2020-09-23	EW	0	19.3	597	8.5	112.8	10.3

Table A3: Additional chemical parameters of the groundwater (GW), the river water (EW), and the distant groundwater (dGW). Concentrations are given in mg l^{-1} if not specified otherwise.

Date	Sample	Distance [m]	DIC	DOC	$KB_{8.2}$ [mmol L^{-1}]	$KS_{4.3}$ [mmol L^{-1}]	K^+	Na^+	Mg^{2+}	Ca^{2+}	SO_4^{2-}	Cl^-	CH_4 [µmol L^{-1}]	CO_2 [µmol L^{-1}]
2020-08-04	GW	1	23	6.9	0.7	3.5	6.1	35	8.6	69	43.5	45.7	17.8	609.7
2020-08-04	GW	3	48	9.3	1.6	3.5	7.1	34	12	78	71.3	46.6	10.6	883.3
2020-08-04	GW	5	49	12.0	2.1	3.6	6.6	32	12	75	66.8	42.8	11.4	1960.1
2020-08-04	GW	6	50	13.5	0.4	3.1	6.7	36	12	73	74.2	53.4	5.7	3681.4
2020-08-04	EW	0	42	13.1	0.0	1.9	6.8	47	9.9	64	78.5	89.8	0.3	13.3
2020-09-02	GW	2	-	-	-	-	-	-	-	-	-	-	57.6	1485.7
2020-09-02	EW	0	-	-	-	-	-	-	-	-	-	-	0.2	32.6
2020-09-07	dGW	2000	35	3.9	0.5	2.8	96	33	14	89	178	60.1	28.9	749.5
2020-09-07	dGW	500	45	2.8	1.0	3.3	3.6	42	14	94	134.9	62.1	0.2	32.6
2020-09-23	GW	1	70	9.4	0.6	4.5	7.4	36	10	81	7.25	60.3	188.7	1193.4
2020-09-23	GW	2	64	9.9	0.8	4.8	7.7	38	11	86	20	68.2	185.7	898.5
2020-09-23	GW	3	64	11.5	1.1	5.3	7.2	36	11	82	31.3	56	212.4	1117.5
2020-09-23	GW	4	55	11.0	1.3	4.7	8.4	35	13	95	92.1	52.1	70.4	1024.3
2020-09-23	EW	0	24	6.3	0.0	1.9	6.8	41	9.4	57	78.8	75.6	2.5	31.6

Table A4: The mean (± SD) $\delta^{13}C$ signatures at the study site for each measurement day.

Date	Sample	$\delta^{13}C$ [‰]	± SD
2020-08-04	Flux	-11,3	0,95
2020-08-04	EW	-18,6	0,79
2020-08-04	GW	-22,3	0,37
2020-08-04	OM	-26,4	0,74
2020-09-02	GW	-22,8	0,46
2020-09-02	EW	-16,5	2,83
2020-09-02	Flux	-15,7	0,17
2020-09-02	OM	-27,4	0,40
2020-09-07	dGW	-18,5	0,19
2020-09-23	EW	-16,4	0,87
2020-09-23	GW	-23,7	0,43
2020-09-23	Flux	-12,9	0,81
2020-09-23	OM	-27,1	0,49
2020-09-23	OM_sat	-26,8	0,86

Table A5: Results of Kruscal-Wallice and Dunn's post-hoc test comparing the mean (± SD) δ13C signatures of the CO_2 flux and the endmembers at the study site.

	Flux_cor	Flux	GW	EW	OM
Flux_cor					
Flux	1.00				
GW	0.61	1.00			
EW	1.00	1.00	1.00		
OM	< 0.01	< 0.01	< 0.01	< 0.01	
OM_sat	< 0.01	< 0.01	0.04	0.01	1.00

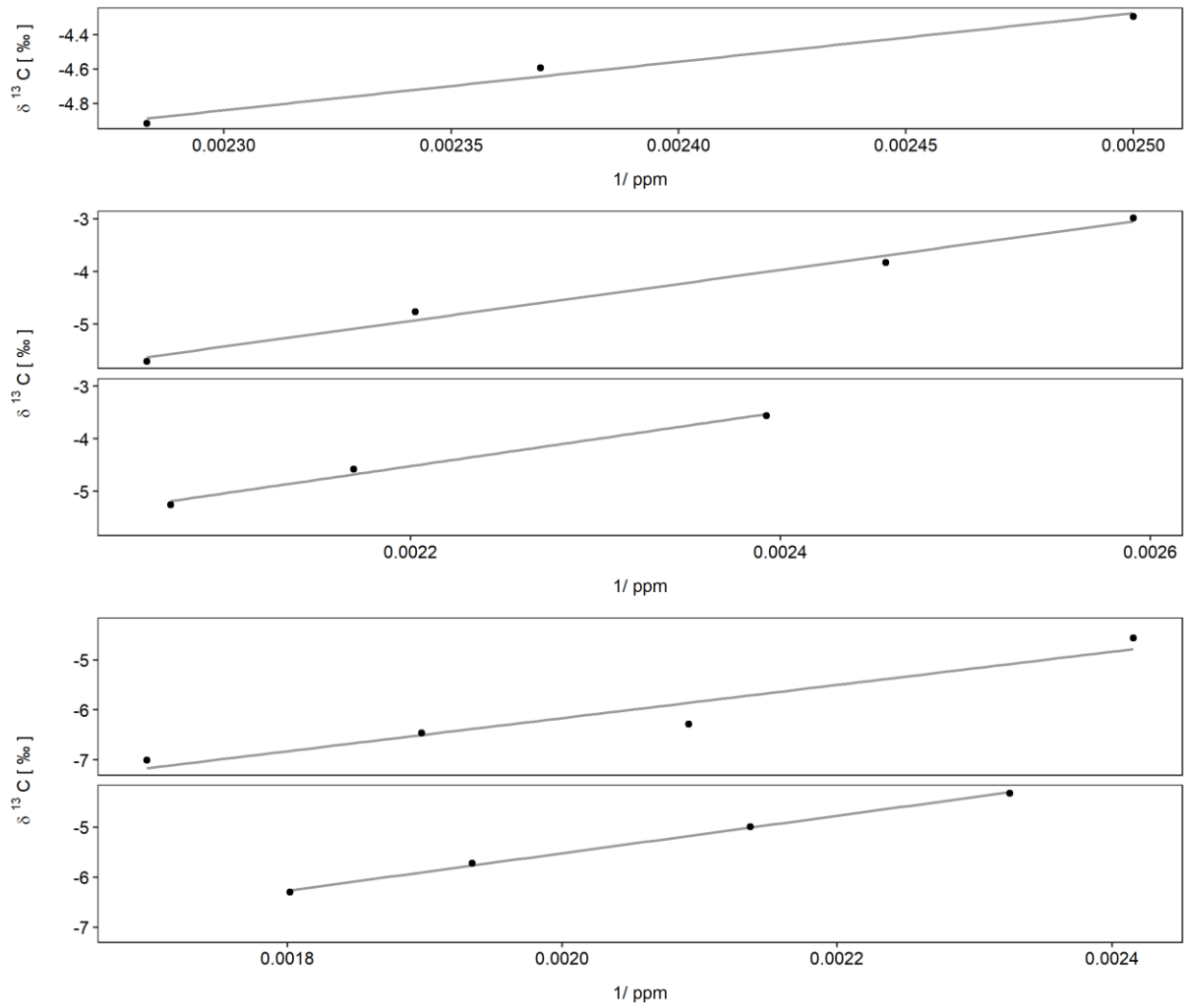

Figure A3: Keeling plots from the 4th of August (top), the 2nd of September (middle) and the 23rd of September (bottom). The $\delta^{13}CO_2$ signatures are plotted against the reciprocal of the concentration.

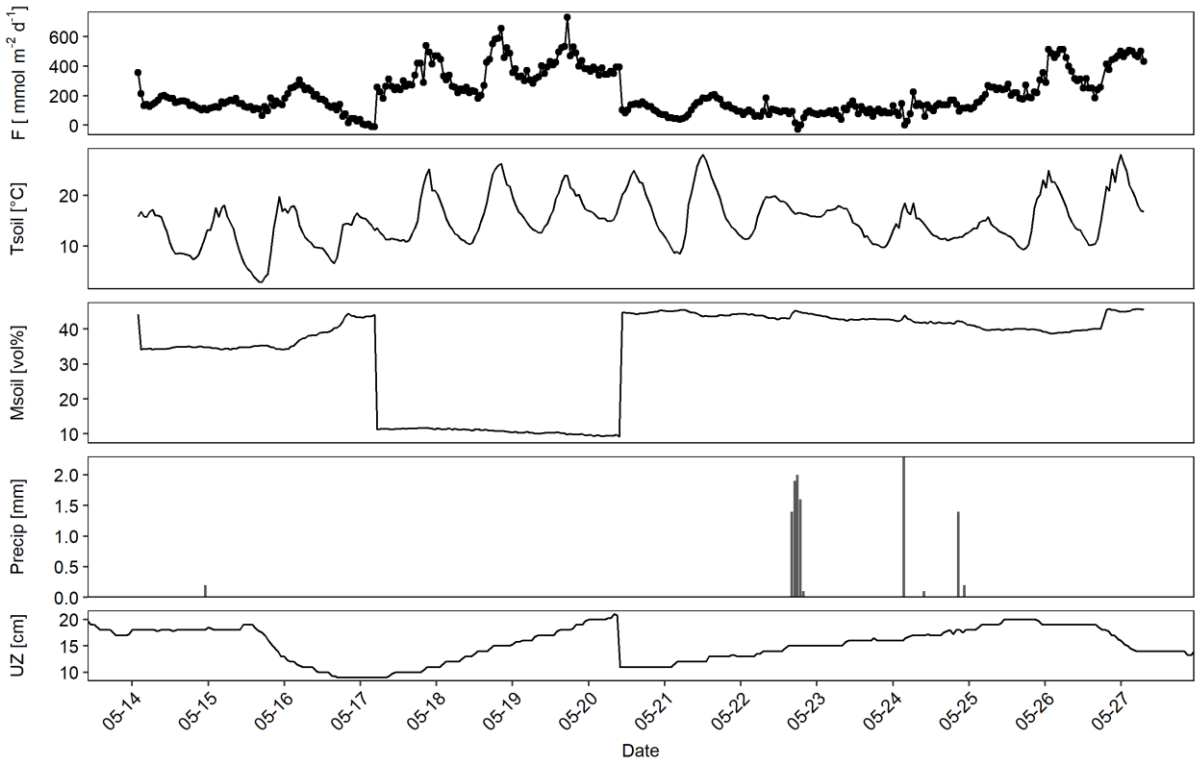

Figure A4: The CO_2 fluxes (F) and the environmental variables soil temperature (Tsoil), soil moisture (Msoil), Precipitation (Precip) and thickness of the unsaturated zone (UZ) from automatic measurements in May.

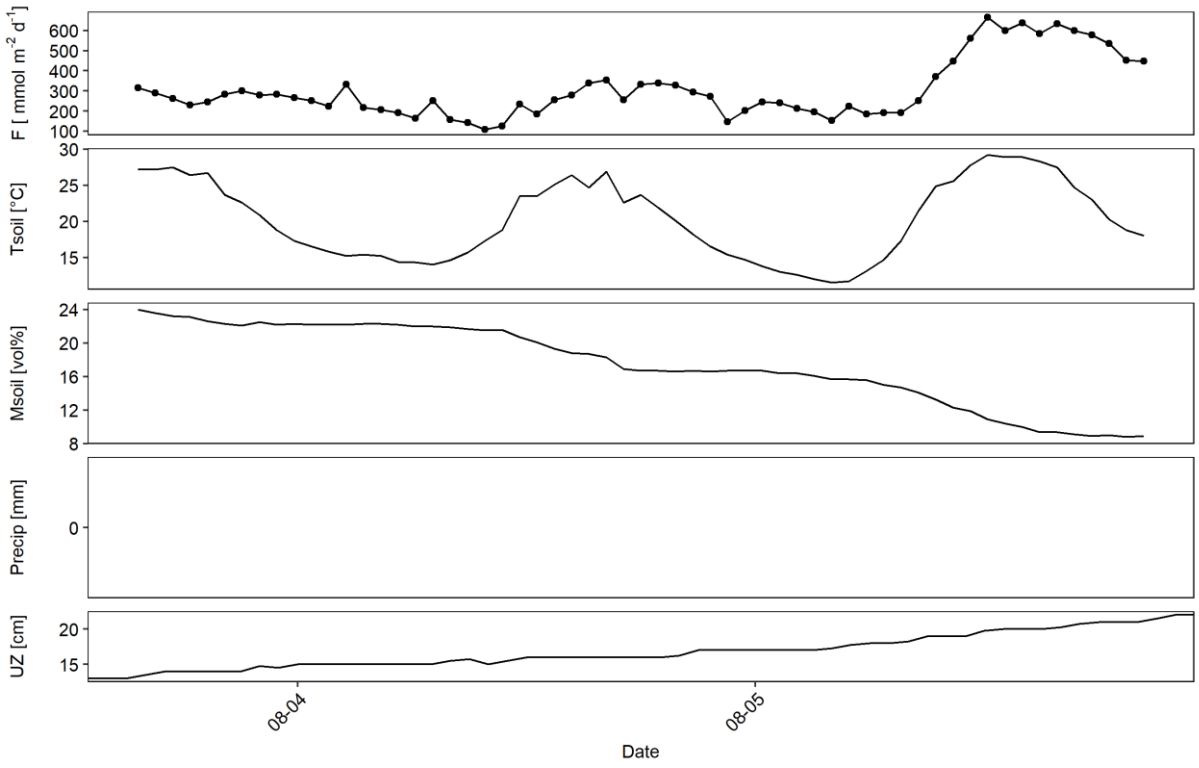

Figure A5: The CO_2 fluxes (F) and the environmental variables soil temperature (Tsoil), soil moisture (Msoil), Precipitation (Precip) and thickness of the unsaturated zone (UZ) from automatic measurements in August.

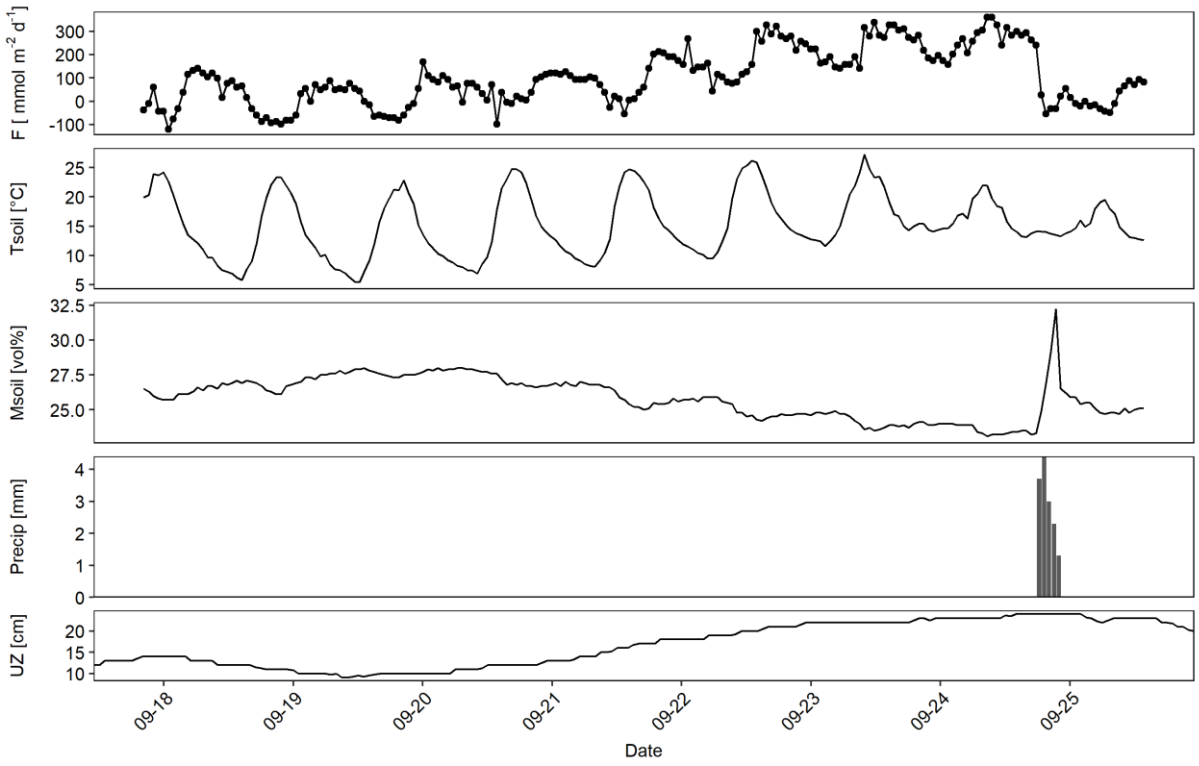

Figure A6: The CO_2 fluxes (F) and the environmental variables soil temperature (Tsoil), soil moisture (Msoil), Precipitation (Precip) and thickness of the unsaturated zone (UZ) from automatic measurements in September.

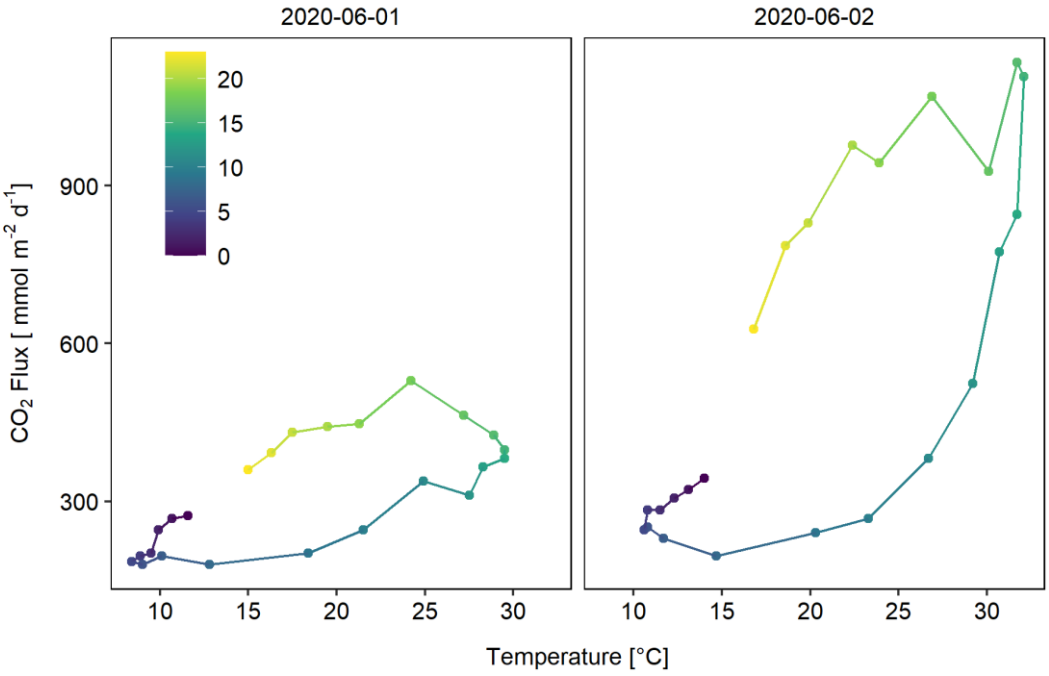

Figure A7: Temperature response of CO2 fluxes on the 1st of June and the 2nd of June. The colors represent the hour of the day.

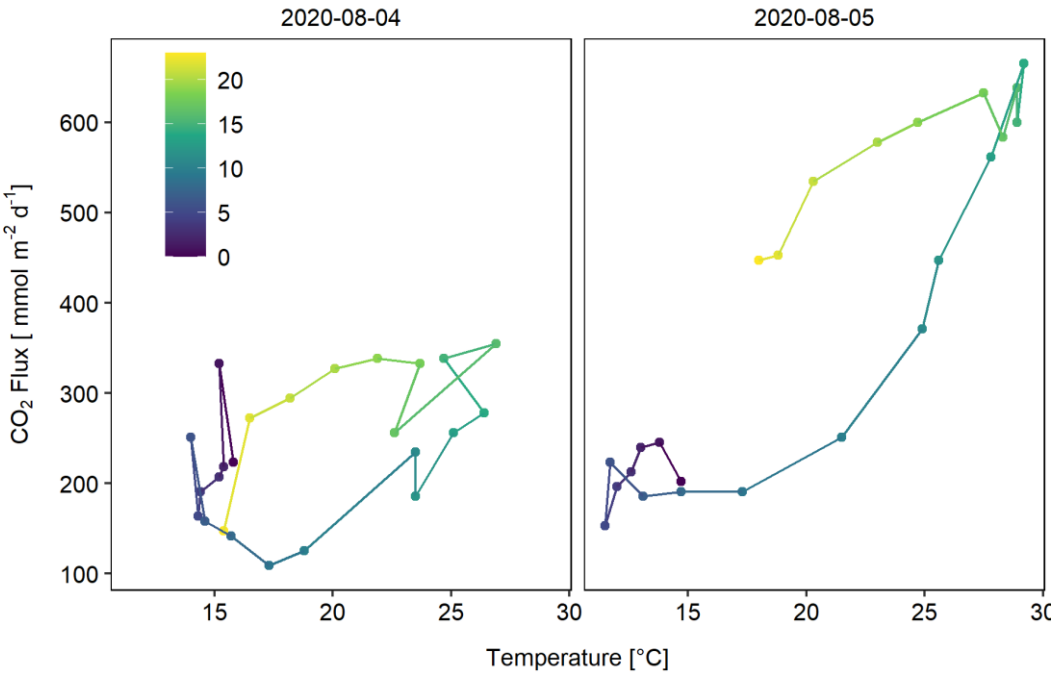

Figure A8: Temperature response of CO2 fluxes on the 4th of August and the 5th of Auguts. The colors represent the hour of the day.

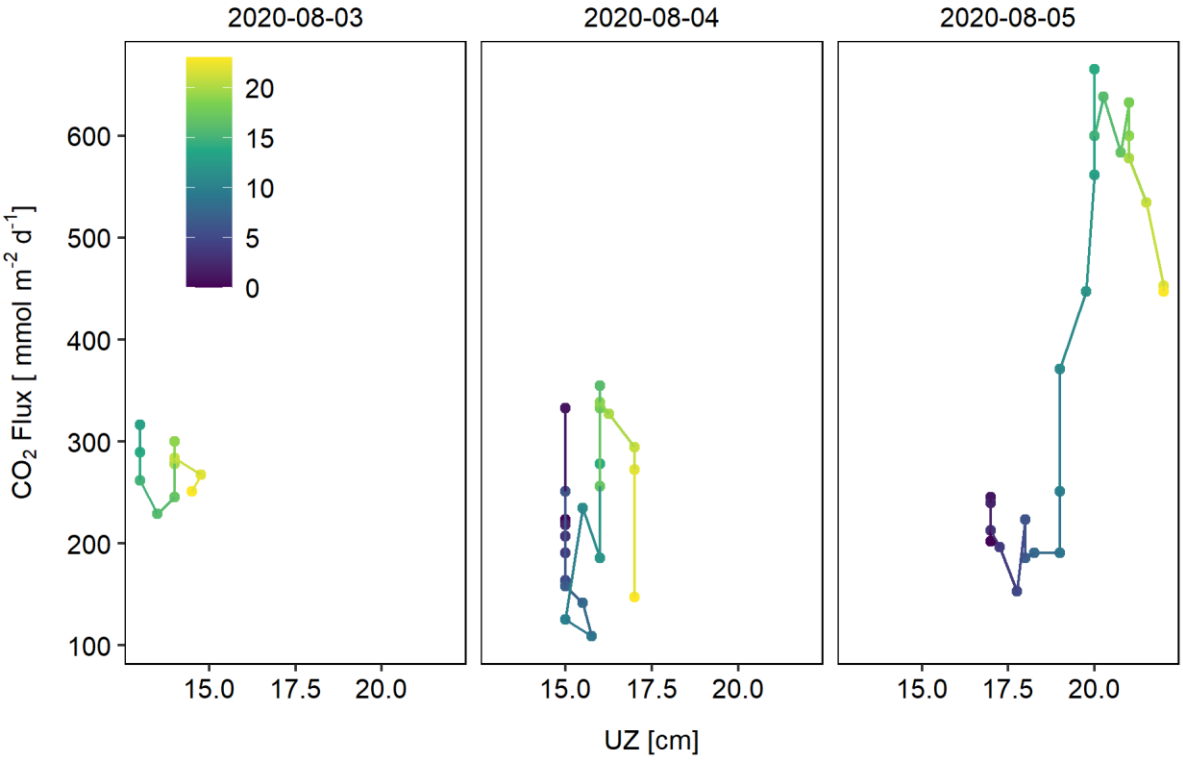

Figure A9: A representative example for the relation of the thickness of the unsaturated zone (UZ) and the CO2 fluxes from the 3rd of August to the 5th of August. The colors represent the hour of the day. No consistent pattern can be observed.

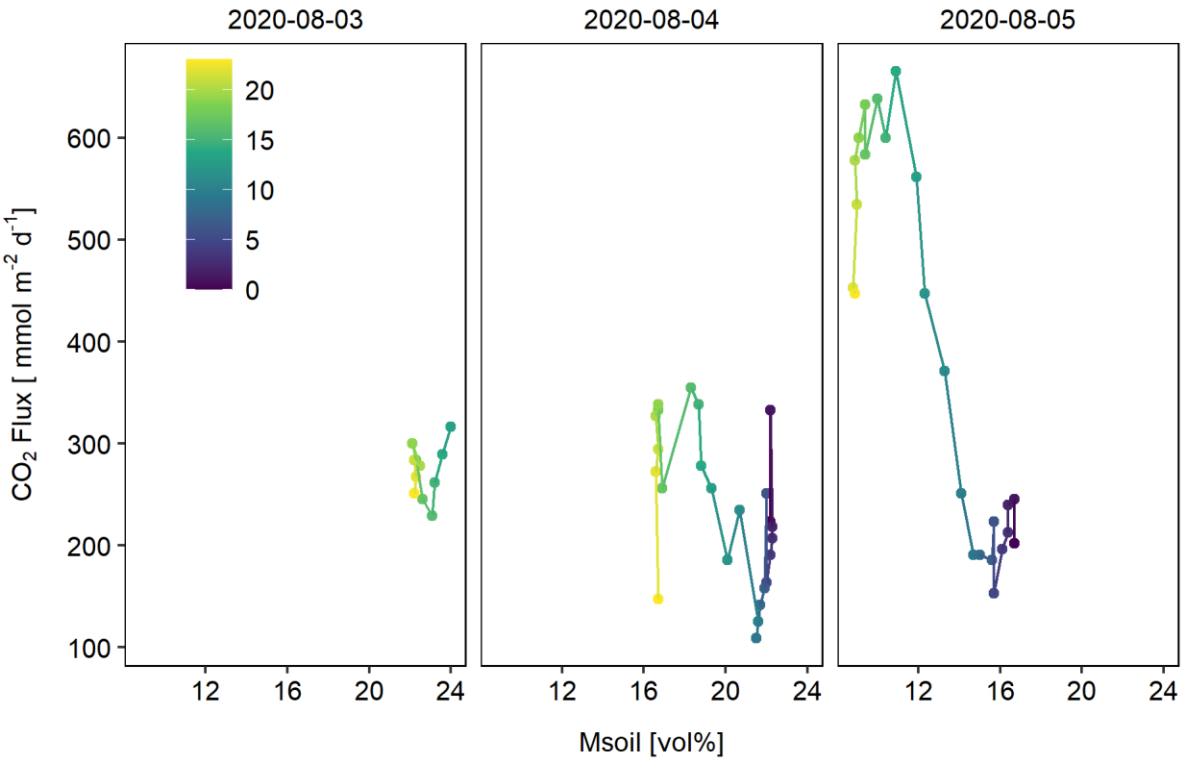

Figure A10: A representative example for the relation of soil moisture (Msoil) and the CO2 fluxes from the 3rd of August to the 5th of August. The colors represent the hour of the day.

Declaration of Academic Integrity

I hereby confirm that this thesis on "Mechanisms of Carbon Dioxide Emissions from Dry Sediments of the River Elbe" is solely my own work and that I have used no sources or aids other than the ones stated. All passages in my thesis for which other sources, including electronic media, have been used, be it direct quotes or content references, have been acknowledged as such and the sources cited.

_____

(date and signature of student)

I agree to have my thesis checked in order to rule out potential similarities with other works and to have my thesis stored in a database for this purpose.

_____

(date and signature of student)